High-Resolution Finite Volume Methods for Acoustics in a Rapidly-Varying Heterogeneous Medium

by

Tiernan Fogarty

A dissertation submitted in partial fulfillment of
the requirements for the degree of

Master of Science

University of Washington

1997

Approved by____

(Chairperson of Supervisory Committee)

____

____

Program Authorized
to Offer Degree____

Date____

In presenting this thesis in partial fulfillment of the requirements for a Master's degree at the University of Washington, I agree that the Library shall make its copies freely available for inspection. I further agree that extensive copying of this thesis is allowable only for scholarly purposes, consistent with "fair use" as prescribed in the U.S. Copyright Law. Any other reproduction for any purposes or by any means shall not be allowed without my written permission.

Signature ______________________________

Date ________________________________

University of Washington

Abstract

High-Resolution Finite Volume Methods for Acoustics in a Rapidly-Varying Heterogeneous Medium

by Tiernan Fogarty

Chairperson of Supervisory Committee
Professor Randall J. LeVeque
Department of Applied Mathematics

Behavior of acoustic waves in a rapidly-varying heterogeneous medium may be investigated analytically via various homogenization theories. Alternatively, one can solve the heterogeneous equations directly with a numerical method. Although a direct numerical solution can be difficult with standard methods, we have found the equations can be solved directly using high-resolution multi-dimensional finite volume methods based on solving "Riemann Problems". These methods have been developed and implemented in the software package CLAWPACK, and applied directly to solve the linear acoustics problem with discontinuous and rapidly-varying material parameters. Numerical solutions of the acoustics equations in this setting are not restricted to any particular arrangement of material parameters. The combination of direct numerical solution techniques with asymptotic homogenization theories provides crucial feedback for testing both numerical methods and homogenization theories.

TABLE OF CONTENTS

LIST OF FIGURES

ACKNOWLEDGMENTS

I would like to thank Professor Randall J. LeVeque for all his help and guidance. I would also like to thank Tricia Burgess and Arnold Kim for their many ideas and endless patience. Finally I would like to thank my parents Tom and Jeri Fogarty.

Chapter 1

ONE DIMENSIONAL LINEAR ACOUSTICS

The purpose of the following investigation is to develop a robust numerical method for solving the acoustics problem. The numerical method will be used both as a verification of the solver in use, CLAWPACK, and as means of providing numerical verification to existing theory. First, it is shown that CLAWPACK reproduces previously known theoretical and numerical behavior of the forward acoustics problem. Next, CLAWPACK is used to explore areas of interest which were previously beyond the reach of numerical models.

The forward acoustics problem may be described as the following: Given a medium with known values of material parameters such as $\rho(x)$ (density) and $\mu(x)$ (bulk modulus), determine the pressure $p(x,t)$ and velocity $u(x,t)$ fields resulting from some initial acoustic disturbance. Here $p(x,t)$ and $u(x,t)$ are the (small amplitude) excess pressure and velocity fields resulting from a perturbation of the background state. The most straight forward example of the forward problem that may be studied is the one-dimensional acoustics problem.

The organization of this paper is as follows. In Sections 1.1-1.3 the one-dimensional acoustics problem and discontinuous media are introduced. Numerical methods of solution are discussed in Section 2. An overview of CLAWPACK and the flux-limiters will be introduced. Sections 3.1-3.2 examine the single interface problem and several interfaces, while Section 3.3 illustrates homogenization theory for a heterogeneous periodic medium. Errors arising in the standard implementation of flux-limiters to a heterogeneous periodic medium are outlined in Section 4.1. The solution method, and the resolution of these errors, are explored in Section 4.2. Order of accuracy of the two limiting methods are discussed in Sections 3.1, 3.2, and 4.2. New applications, including non-dispersive heterogeneous medium and random medium, are discussed in Sections 5.1 and 5.2. Finally we will outline areas of future work and summarize the presentation in Section 6.

1.1 Conservation Law

We will be investigating the forward problem for one-dimensional acoustics. The governing equations may be derived via a conservation law, which in one space dimension takes the form, (see [11])

$$\frac{\partial}{\partial t}q(x,t) + \frac{\partial}{\partial x}f(q(x,t)) = 0. \tag{1.1}$$

Here $q(x,t)$ is an m-dimensional vector of conserved quantities, or state variables, e.g. mass, momentum, etc. Thus q_j is the density function for the jth state variable, where the total quantity of q_j in the interval $[x_1, x_2]$ at time t is defined as $\int_{x_1}^{x_2} q_j(x,t)dx$. We assume that the variables q_j are conserved quantities, thus $\int_{-\infty}^{\infty} q_j(x,t)dx$ should be constant with respect to t. Consequently if we are in the interval $[x_1, x_2]$, then

$$\frac{\partial}{\partial t}\int_{x_1}^{x_2} q_j(x,t)dx = F_1(t) - F_2(t). \tag{1.2}$$

Since the quantities q_j are conserved within $[x_1, x_2]$, changes in q_j within this interval must be the result of $F_1(t)$ and $-F_2(t)$, which represent fluxes into the interval.

If we have a flux which is only dependent on $q(x,t)$, then we can rewrite (1.2) as

$$\frac{\partial}{\partial t}\int_{x_1}^{x_2} q_j(x,t)dx = f(q(x_1,t)) - f(q(x_2,t)). \tag{1.3}$$

If we make the further assumption that q and f are smooth functions then (1.3) becomes

$$\frac{\partial}{\partial t}\int_{x_1}^{x_2} q_j(x,t)dx = \int_{x_1}^{x_2} \frac{\partial}{\partial x} f(q(x,t))dx, \tag{1.4}$$

which can be rewritten as

$$\int_{x_1}^{x_2} [\frac{\partial}{\partial t} q_j(x,t)dx \ + \ \frac{\partial}{\partial x} f(q(x,t))]dx = 0. \tag{1.5}$$

Since (1.5) must be true for all intervals $[x_1, x_2]$, the integrand must be zero, which recovers (1.1):

$$\frac{\partial}{\partial t} q(x,t) + \frac{\partial}{\partial x} f(q(x,t)) = 0. \tag{1.6}$$

1.2 Linearization

For the acoustics problem we are interested in acoustic waves propagating through a compressible medium. These waves, which are disturbances in the background state of the medium, have such small amplitude that products or powers of the disturbance, or perturbation, amplitude may be ignored. The assumption of very small amplitude allows us to study acoustic perturbations as a linear phenomena.

In order to study acoustic waves as a linear phenomena we must first derive the governing equations for the system and then linearize about some background state. If we consider equation (1.6) with variable $u(x,t)$ and $\rho(x,t)$ we find the conservation law for ρ as

$$\frac{\partial}{\partial t}\rho(x,t) + \frac{\partial}{\partial x}(\rho(x,t)u(x,t)) = 0, \tag{1.7}$$

often called the continuity equation. Although velocity is not a conserved quantity, the momentum is, so we must derive an equation for the conservation of momentum to characterize the velocity. If we let $P(x,t) = \rho(x,t)u(x,t)$ describe the density of momentum, then in the absence of any outside forces we may define the momentum flux as

$$\text{momentum flux} = (\rho(x,t)u(x,t))u(x,t) + p(x,t).$$

This gives the conservation law for the momentum as

$$\frac{\partial}{\partial t}(\rho(x,t)u(x,t)) + \frac{\partial}{\partial x}(\rho(x,t)u^2(x,t) + p(x,t)) = 0. \tag{1.8}$$

We now consider flow which is isentropic, i.e. the entropy of the gas is constant. For isentropic flow we have an equation of state which gives the pressure in terms of the density as

$$p = \kappa\rho^\gamma,$$

where κ and γ are constants specified by the given medium. We can combine the equation of state with our equations for conserved quantities, equations (1.7) and (1.8), to derive the conservation laws for isentropic flow as

$$\frac{\partial}{\partial t}\rho + \frac{\partial}{\partial x}(\rho u) = 0$$

and

$$\frac{\partial}{\partial t}(\rho u) + \frac{\partial}{\partial x}(\rho u^2 + \kappa\rho^\gamma) = 0.$$

If we define

$$q = \begin{bmatrix} \rho \\ \rho u \end{bmatrix} = \begin{bmatrix} q_1 \\ q_2 \end{bmatrix}, \text{ and } f(q) = \begin{bmatrix} \rho u \\ \rho u^2 + \kappa \rho^\gamma \end{bmatrix} = \begin{bmatrix} q_2 \\ q_2^2/q_1 + \kappa q_1^\gamma \end{bmatrix},$$

we can write our system of conservation laws as

$$\frac{\partial}{\partial t}(q) + \frac{\partial}{\partial x}(f(q)) = 0. \tag{1.9}$$

Given the conservation law (1.9), we can linearize the system about some background state q_0 by defining the perturbed state $\tilde{q}$, in terms of the background state q_0 as

$$q(x,t) = q_0 + \tilde{q}(x,t). \tag{1.10}$$

To linearize we substitute (1.10) into (1.6) and discard terms involving powers or products of $\tilde{q}$. This leads to the linearized equations

$$\tilde{q}_t + f'(q_0)\tilde{q}_x = 0,$$

where $f'(q_0)$ is the Jacobian matrix given by

$$f'(q_0) = \begin{bmatrix} \partial f_1/\partial q_1 & \partial f_1/\partial q_2 \\ \partial f_2/\partial q_1 & \partial f_2/\partial q_2 \end{bmatrix}\Bigg|_{q=q_0} = \begin{bmatrix} 0 & 1 \\ -u_0^2 + \gamma p_0/\rho_0 & 2u_0 \end{bmatrix}. \tag{1.11}$$

If we linearize around $u_0 = 0$, and some fixed p_0, we find the linearized continuity and momentum equations are

$$\tilde{\rho}_t + (\tilde{\rho}\tilde{u})_x = 0 \tag{1.12}$$

and

$$(\tilde{\rho}\tilde{u})_t + (\gamma p_0/\rho_0)(\tilde{\rho}\tilde{u})_x = 0. \tag{1.13}$$

We know that $p = \kappa\rho^\gamma$, thus we have

$$p = p_0 + \tilde{p} = \kappa(\rho_0 + \tilde{\rho})^\gamma$$

$$= \kappa\rho_0^\gamma + \gamma\kappa\rho_0^{\gamma-1}\tilde{\rho} + \cdots .$$

This gives

$$\tilde{p} = (\gamma p_0/\rho_0)\tilde{\rho} + \text{ (higher order terms)}.$$

For linear theory we discard the higher order terms. This gives the perturbed pressure as

$$\tilde{p} = c_0^2\tilde{\rho}, \tag{1.14}$$

with sound speed c_0, defined as $c_0 = \sqrt{\gamma p_0/\rho_0}$. We can substitute (1.14) into (1.12) and (1.13) to find

$$\begin{bmatrix} \tilde{p} \\ \tilde{u} \end{bmatrix}_t + \begin{bmatrix} 0 & \gamma p_0 \\ 1/\rho_0 & 0 \end{bmatrix} \begin{bmatrix} \tilde{p} \\ \tilde{u} \end{bmatrix}_x = 0.$$

For elastic solids the acoustics equations can be written in the same form where $\mu_0 = \gamma p_0$ is the "bulk modulus of elasticity". This gives the linear acoustics equations in elastic solids as

$$\begin{bmatrix} p \\ u \end{bmatrix}_t + \begin{bmatrix} 0 & \mu_0 \\ 1/\rho_0 & 0 \end{bmatrix} \begin{bmatrix} p \\ u \end{bmatrix}_x = 0. \tag{1.15}$$

1.3 Heterogeneous medium

In a heterogeneous medium we may have the material parameters ρ (density) or μ (bulk modulus) change with location x. As these parameters are not constant we can no longer have a conservation law, but rather a variable-coefficient hyperbolic system

$$q_t + A(x)q_x = 0, \tag{1.16}$$

where

$$q = \begin{bmatrix} p \\ u \end{bmatrix}, \quad A = \begin{bmatrix} 0 & \mu(x) \\ 1/\rho(x) & 0 \end{bmatrix}. \tag{1.17}$$

This lack of strict conservation form will be addressed in Sections 2.1 and 6.1. CLAWPACK can still be applied, following [9] and [12].

In the setting of CLAWPACK, we have cells between the grid points x_i and x_{i+1}. Here the ith cell has material parameters ρ_i and μ_i. We set

$$A_i = \begin{bmatrix} 0 & \mu_i \\ 1/\rho_i & 0 \end{bmatrix}, \tag{1.18}$$

with the sound speed in the ith cell given by $c_i = \sqrt{\mu_i/\rho_i}$. The system can be diagonalized to find

$$R = \begin{bmatrix} r_i^1 & r_i^2 \end{bmatrix} = \begin{bmatrix} -c_i & c_i \\ 1/\rho_i & 1/\rho_i \end{bmatrix}, \quad \Lambda = \begin{bmatrix} -c_i & 0 \\ 0 & c_i \end{bmatrix}, \quad R^{-1} = \frac{\rho_i}{2c_i} \begin{bmatrix} -1/\rho_i & c_i \\ 1/\rho_i & c_i \end{bmatrix}. \tag{1.19}$$

Here the eigenvalues of $A(x)$ are the wave speeds $\lambda_i^1 = -c_i$ and $\lambda_i^2 = +c_i$.

We would like to have the interface between layers of different media to be at a grid point. Given material parameters which depend on the spatial variable (e.g. $\mu(x), \rho(x)$ etc.) we would like to define these properties accurately in each cell, and thus between the interfaces. To accomplish this we define the midpoint of each grid point as $\bar{x}_i = (x_{i+1} + x_i)/2$, which allows us to redefine $A(x)$ as

$$A_i = A(\bar{x}_i) = \begin{bmatrix} 0 & \mu(\bar{x}_i) \\ 1/\rho(\bar{x}_i) & 0 \end{bmatrix} = \begin{bmatrix} 0 & \mu_i \\ 1/\rho_i & 0 \end{bmatrix}.$$

Alternatively we could set ρ_i to the cell average of $\rho(x)$ and μ_i to the harmonic average of $\mu(x)$. This formulation allows spatially varying parameters to be represented numerically as piecewise constant functions. For example, the value of ρ in the ith cell would be $\rho_i = \rho(\bar{x}_i)$ where $\rho(\bar{x}_i)$ is the average value of $\rho(x)$ in the ith cell

$$\rho_i = (1/h) \int_{x_i}^{x_{i+1}} \rho(x) dx.$$

Note that we could rewrite (1.15) as

$$\begin{bmatrix} 1/\mu_0 & 0 \\ 0 & \rho_0 \end{bmatrix} \begin{bmatrix} p \\ u \end{bmatrix}_t + \begin{bmatrix} 0 & 1 \\ 1 & 0 \end{bmatrix} \begin{bmatrix} p \\ u \end{bmatrix}_x = 0. \qquad (1.20)$$

This is the same system but written in what is known as capacity-form. We will return to a discussion of capacity-form in Section 6.1.

Chapter 2

NUMERICS VIA CLAWPACK

2.1 Clawpack

CLAWPACK (Conservation LAWs PACKage) is a collection of Fortran subroutines for solving hyperbolic systems of conservation laws in one and two space dimensions, both with and without source terms. High resolution flux-limiter finite volume methods are used on uniform rectangular grids. See [8] and [12] for details.

In one space dimension, the conservation law has the form

$$\frac{\partial}{\partial t}q(x,t) + \frac{\partial}{\partial x}f(q(x,t)) = 0$$

where q is the vector of conserved quantities. CLAWPACK is formulated so that it can be applied to systems which are not in strict conservation form, e.g., variable-coefficient systems, discussed previously. CLAWPACK is a finite volume method based on the solving of a Riemann problem at each grid point in order to calculate the left and right going fluctuations. See [12] for details.

If we consider the cell average in the interval $[x_i, x_{i+1}]$, we must have constant values of material parameters. In neighboring intervals, although we may have different values, values of the material parameters must also be constant. Thus at each grid point x_i we have a classic Riemann problem: the hyperbolic equation with piecewise constant initial data

$$q(x_i, 0) = \begin{cases} q_l, & \text{if } x < x_i, \\ q_r, & \text{if } x > x_i. \end{cases}$$

For each interval $[x_i, x_{i+1}]$, there is defined a matrix A_i which contains the constant values of the material parameters in the interval. At each grid point there is a Riemann problem consisting of the state q_{i-1} in cell $i-1$, to the left, and the state q_i in cell i, to the right. The solution to this Riemann problem consists of a left and right-going wave. The left-going wave moves into cell $i-1$ with speed $\lambda^1_{i-1} = -c_{i-1}$ and the right-going wave moves into cell i with speed $\lambda^2_i = c_i$. The jump across the left-going wave must be a scalar multiple of the eigenvector r^1_{i-1} of the matrix A_{i-1} (see equation (1.19))

$$\mathcal{W}^1_i = \alpha^1_i \begin{bmatrix} -c_{i-1} \\ 1/\rho_{i-1} \end{bmatrix},$$

and the jump across the right-going wave must be a scalar multiple of the eigenvector r^2_i of the matrix A_i

$$\mathcal{W}^2_i = \alpha^2_i \begin{bmatrix} c_i \\ 1/\rho_i \end{bmatrix},$$

for some scalars α^1_i and α^2_i. The state between the two waves must be continuous across the interface

$$q_{i-1} + \mathcal{W}^1_i = q_i + \mathcal{W}^2_i,$$

so that the wave strengths α^1_i and α^2_i can be found as

$$\alpha^1_i = (-\bigtriangleup q^1/\rho_i + c_i \bigtriangleup q^2)/(c_{i-1}/\rho_i + c_i/\rho_{i-1}),$$

$$\alpha_i^2 = (\triangle q^1/\rho_{i-1} + c_{i-1} \triangle q^2)/(c_{i-1}/\rho_i + c_i/\rho_{i-1}),$$

where $\triangle q$ is defined as

$$\triangle q = \begin{bmatrix} p_i - p_{i-1} \\ u_i - u_{i-1} \end{bmatrix} = \begin{bmatrix} \triangle q^1 \\ \triangle q^2 \end{bmatrix}.$$

Following [12], we now introduce "fluctuations"

$$\mathcal{A}^+ \triangle q_i = \lambda_i^2 \mathcal{W}_i^2$$

$$\mathcal{A}^- \triangle q_{i+1} = \lambda_i^1 \mathcal{W}_{i+1}^1.$$

The first-order Godunov method for this problem can be written as

$$\bar{q}_i = q_i - \frac{\triangle t}{\triangle x}(\mathcal{A}^+ \triangle q_i + \mathcal{A}^- \triangle q_{i+1}). \tag{2.1}$$

This method is motivated by Godunov's method (also known as the upwind method).

Introducing a correction flux F_i (in the absence of flux limiters, see Section 2.2) as

$$F_i = \frac{1}{2} \sum_{p=1}^{M_w} |\lambda_i^p|(1 - \frac{\triangle t}{\triangle x}|\lambda_i^p|)\mathcal{W}_i^p,$$

Godunov's method (2.1) can be extended to a high resolution method (see Section 2.2)

$$\bar{q}_i = q_i - \frac{\triangle t}{\triangle x}(\mathcal{A}^+ \triangle q_i + \mathcal{A}^- \triangle q_{i+1}) - \frac{\triangle t}{\triangle x}(F_{i+1} - F_i) \tag{2.2}$$

which reduces to the standard Lax-Wendroff method if $A_i = \mathcal{A}$ is constant. See [11] and [12] for more details. Equation (2.2) is the form of the update formula used in the CLAWPACK software.

2.2 Flux-limiters

A high-resolution method is a second order accurate method, e.g., Lax-Wendroff, to which a flux-limiter is added in order to help curtail the appearance of spurious oscillations associated with second order methods. The Lax-Wendroff method can work well if q has no steep gradients or discontinuities. However, if some sort of limiting is performed in regions of steep gradients then much better performance can be achieved, see [10] for details. Equation (2.2) can be decomposed into the Godunov (upwind) flux plus a correction term:

$$F^{LW}(q_i) = F^{up}(q_i) - \frac{\triangle t}{\triangle x}(F_{i+1} - F_i)$$

$$= F^{up}(q_i) - \frac{\triangle t}{2 \triangle x}\left(\sum_{p=1}^{M_w} |\lambda^p_{i+1}|(1 - \frac{\triangle t}{\triangle x}|\lambda^p_{i+1}|)\mathcal{W}^p_{i+1} - \sum_{p=1}^{M_w} |\lambda^p_i|(1 - \frac{\triangle t}{\triangle x}|\lambda^p_i|)\mathcal{W}^p_i\right). \tag{2.3}$$

To clarify the proper way to limit (2.3), consider the Lax-Wendroff method applied to the one-dimensional constant-coefficient advection equation

$$q_t + uq_x = 0 \text{ (or in conservation form) } q_t + f(q)_x = 0, \quad f(q) = uq.$$

Applying Lax-Wendroff we find

$$F^{LW}(q_i) = F^{up}(q_i) + \frac{1}{2}|u|(1 - \frac{\triangle t}{\triangle x}|u|)(q_i - q_{i-1}). \tag{2.4}$$

The upwind method is excessively numerically dissipative while the correction terms introduced by the Lax-Wendroff method tend to be numerically dispersive. These characteristics suggest a limiting method, which favors the full Lax-Wendroff method in regions where q is smooth (locally), and reduces to, or at least favors, the upwind method when q has steep gradients or discontinuities (locally). A simple way to introduce such a limiter is to alter (2.4) as

$$F^{LW}(q_i) = F^{up}(q_i) + \frac{1}{2}|u|(1 - \frac{\triangle t}{\triangle x}|u|)(q_i - q_{i-1})\Phi_i, \tag{2.5}$$

where Φ_i is the limiter depending on the nature of the solution locally. Note that if $\Phi_i = 0$ then (2.5) is reduced to the upwind method, while if $\Phi_i = 1$ (2.5) is the full Lax-Wendroff method.

If the speed u at q_i is positive, then there is flux incoming from the left, $(i-1)$ while if u is negative there is flux incoming from the right $(i+1)$. Thus limiters should have the form

$$\Phi_i = \phi(\theta_i), \qquad \theta_i = \frac{q_I - q_{I-1}}{q_i - q_{i-1}}, \tag{2.6}$$

where

$$I = \begin{cases} i-1, & \text{if } u > 0 \\ i+1, & \text{if } u \leq 0. \end{cases} \tag{2.7}$$

Although the results achieved in Section 4 will generalize to the superbee, van Leer, and monotonized centered limiters, the limiter used in the following sections will be the "minmod":

$$\text{minmod:} \quad \phi(\theta) = \max(0, \ \min(1, \theta)). \tag{2.8}$$

In order to properly apply the preceding argument to the more general form of the Lax-Wendroff method (2.3), the waves $\mathcal{W}_i^p$ must be limited in amplitude. Each $\mathcal{W}_i^p$ must be replaced by a limited version $\tilde{\mathcal{W}}_i^p$, obtained by comparing $\mathcal{W}_i^p$ with $\mathcal{W}_{i-1}^p$ or $\mathcal{W}_{i+1}^p$ in the context of (2.7). I.e. if $\lambda_i^p > 0$ then $I = i-1$, and if $\lambda_i^p < 0$ then $I = i+1$. For the acoustics equations, where $\mathcal{W}_i^p = \alpha_i^p r_i^p$, we can apply the limiter to the scalars α_i^p and set $\tilde{\mathcal{W}}_i^p = \tilde{\alpha}_i^p r_i^p$, with $\tilde{\alpha}_i^p$ as the limited wave strength. In this setting (for $\lambda_i^p > 0$) we have

$$\tilde{\mathcal{W}}_i^p \;=\; \phi(\theta_i^p)\mathcal{W}_i^p,$$

with (2.6) replaced by

$$\theta_i^p \;=\; \frac{W_{i-1}^p \cdot W_i^p}{W_i^p \cdot W_i^p}, \qquad (2.9)$$

where $\cdot$ is an inner product.

To limit the wave $\mathcal{W}_i^p$, we project it onto the corresponding wave in the upwind direction and normalize. We then limit the strength of the wave via (2.8). Usually this method of limiting works very well.[12] In fact all of the figures 3.1-3.19 were generated with the method of limiting just described. As we can see in all but figure 3.19, the method has been a complete success. In figures 3.16-3.19 we see that, although the method is initially successful, by the time the pulse has propagated several pulse widths a numerical artifact arises which completely degrades the pulse. In the next section we will discuss the solution to this problem via alterations to the limiting method.

Chapter 3

DISCONTINUOUS MEDIA

3.1 The Single Interface

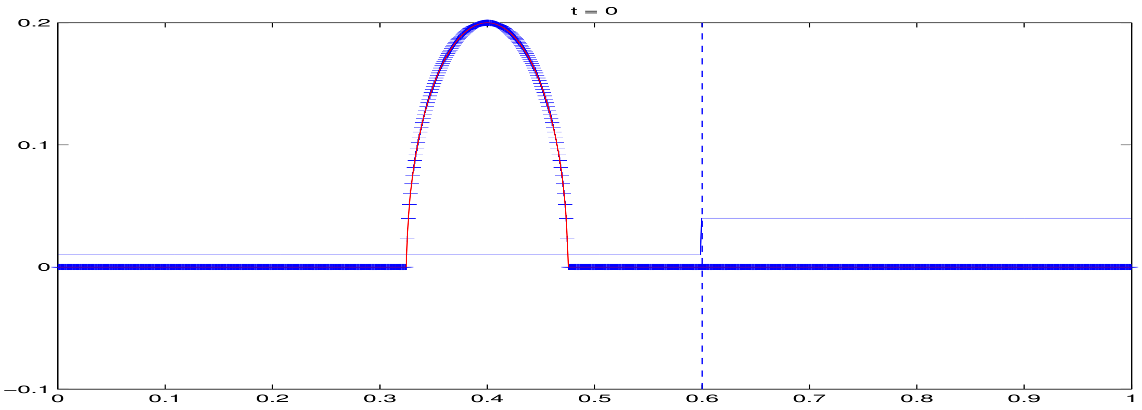

Figure 3.1: true solution(-) and numerical solution (+), time=0, N=1000.

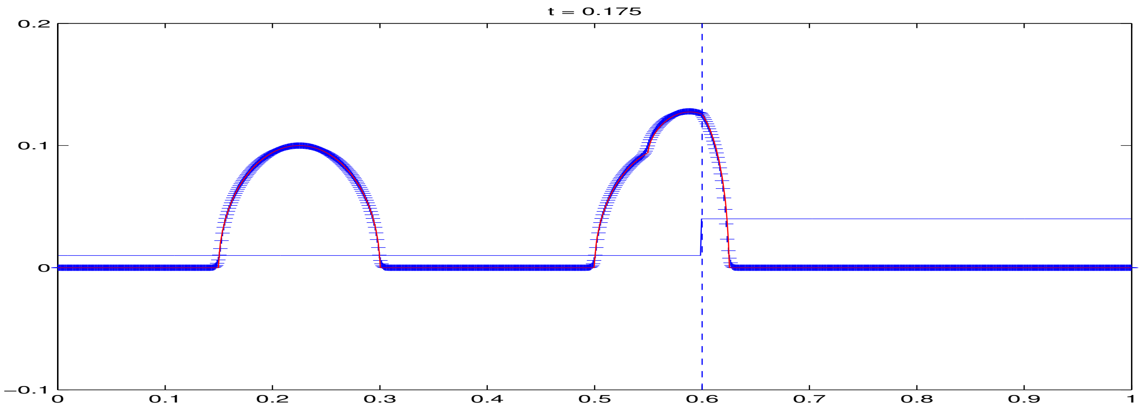

Figure 3.2: true solution(-) and numerical solution (+), time=0.175, N=1000.

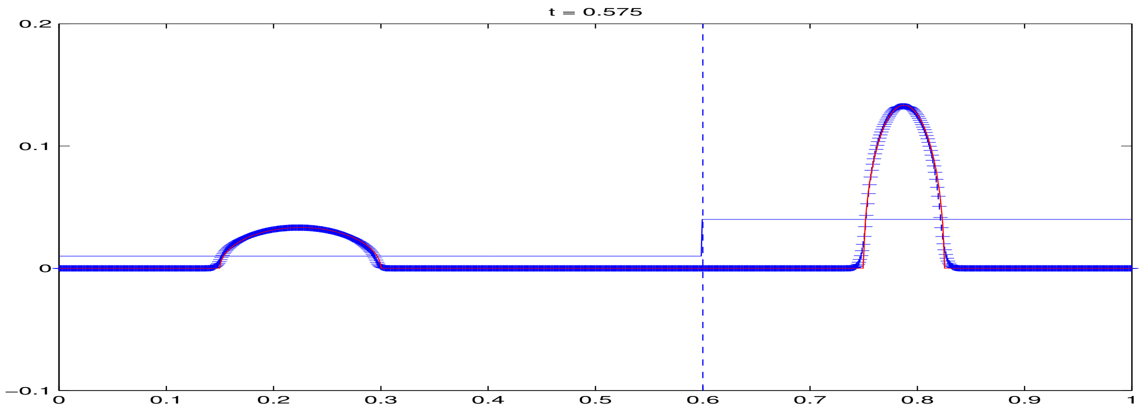

Figure 3.3: true solution(-) and numerical solution (+), time=0.575, N=1000.

We first consider a 1-dimensional problem with a single discontinuity in the density. The medium to the left of the interface is characterized by material parameters ρ_1, μ_1, and c_1 while the medium on the right is characterized by ρ_2, μ_2, and c_2. Thus a wave propagating in either medium can be characterized by an impedance Z where $Z_1 = \rho_1 c_1$ and $Z_2 = \rho_2 c_2$ are the characteristic wave impedances (see [3] for details). Note that Z_1 is defined by the medium that the wave is in before hitting the interface. I.e. for a right-going wave, Z_1 is the impedance of the medium to the left of the interface and Z_2 is the impedance of the medium to the right of the interface. We find the amplitude of reflection and transmission (refraction) coefficients to be

$$R_a = \frac{Z_2 - Z_1}{Z_2 + Z_1} \text{ and } T_a = \frac{2Z_2}{Z_2 + Z_1}. \tag{3.1}$$

These coefficients determine the exact solution of the single interface problem. CLAWPACK is used to solve the interface problem and check against the true solution. Figures 3.1-3.3, show that CLAWPACK gives an excellent solution to the single interface problem. These figures show the numerical solution as '+' and the exact solution as a solid line with a resolution of 1000 grid points in the interval $[0, 1]$. Given that CLAWPACK appears to correctly solve the single interface problem we would like to know the order of accuracy of the numerical method.

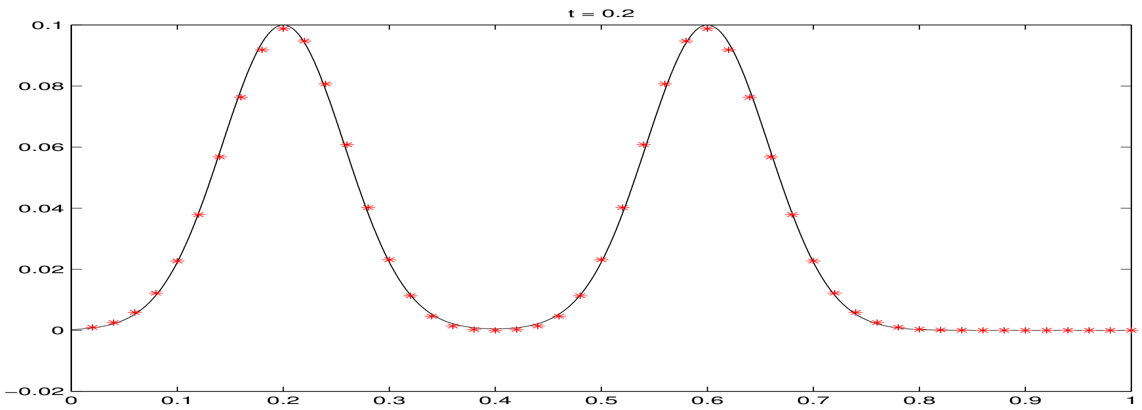

Figure 3.4: $\triangle t < \triangle x$ No limiters used, numerical solutions shown for N=50, compared with numerical "reference" solution at N=1600 (solid line). Smooth data with no discontinuities (i.e. no interfaces).

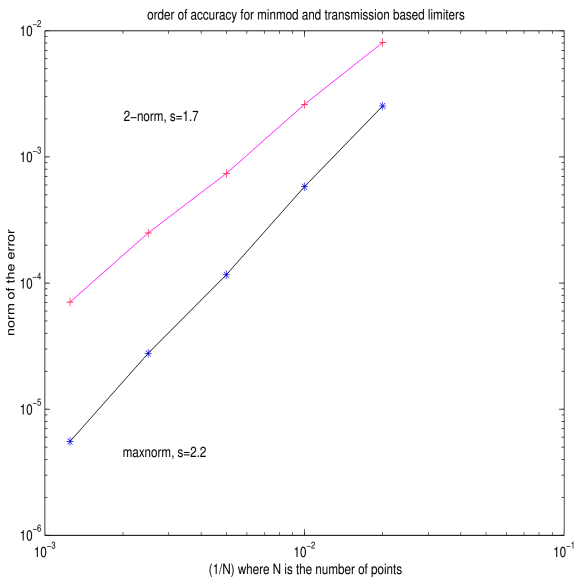

Figure 3.5: Order of accuracy for numerical solutions of figure 3.4. N=50,100,200,400,800 are compared with numerical solution at N=1600, 2-norm and max-norm shown as (+, 2-norm) and (*,max-norm), 2nd order accurate.

Theory predicts that for smooth data, without the use of limiters and in the absence of discontinuities, CLAWPACK should be second-order accurate. Figure 3.5 shows that for the conditions just described (see figure 3.4), CLAWPACK is second-order accurate. We also expect that when flux-limiters are used, even with smooth data and no discontinuities in the medium, the method should be closer to first order accurate.

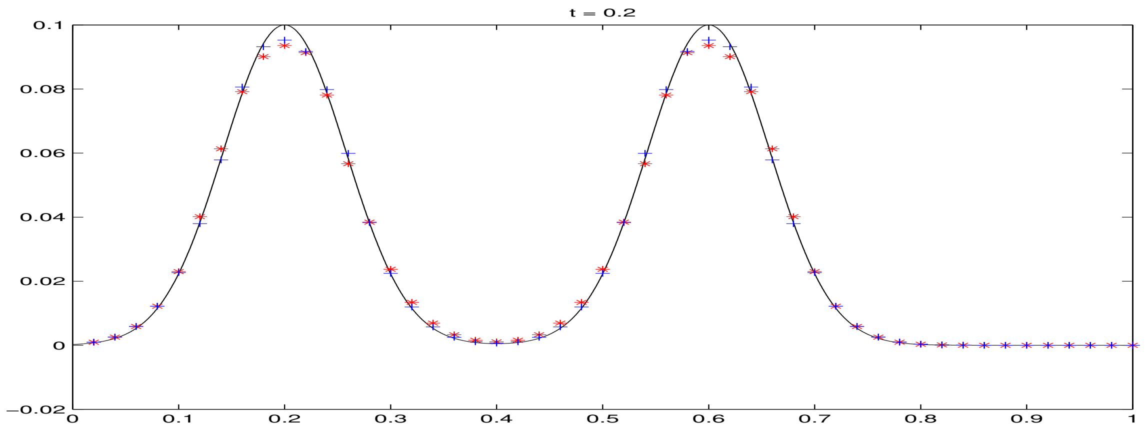

Figure 3.6: $\triangle t < \triangle x$ original and modified limiters used, numerical solutions shown for N=50, original(+) and modified(*) methods, compared with numerical "reference" solution at N=1600 (solid line). Smooth data with no discontinuities (i.e. no interfaces).

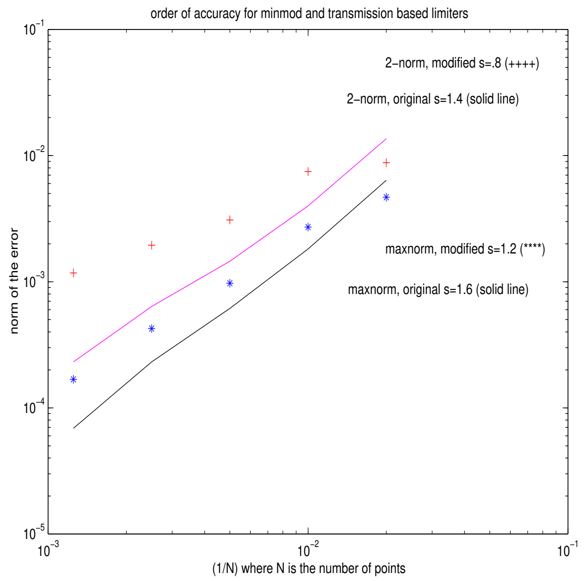

Figure 3.7: Order of accuracy for numerical solutions of figure 3.6. N=50,100,200,400,800 are compared with numerical solution at N=1600, 2-norm and max-norm shown for both methods of limiting, original shown as solid line order of accuracy 1.4 - 1.6, modified shown as (+, 2-norm) and (*,max-norm) order of accuracy .8 - 1.2.

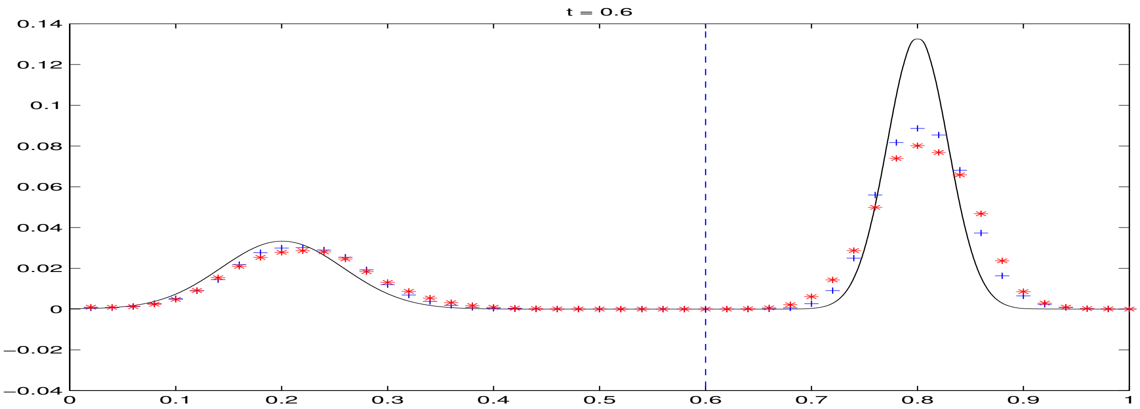

Figure 3.8: $\triangle t < \triangle x$ original and modified limiters used, numerical solutions shown for N=50, original(+) and modified(*) methods, compared with numerical “reference” solution at N=1600 (solid line).

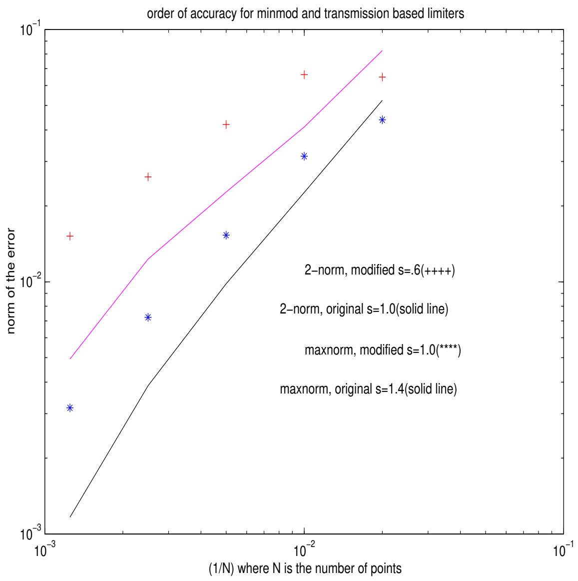

Figure 3.9: Order of accuracy for numerical solutions of figure 3.6. N=50,100,200,400,800 are compared with numerical solution at N=1600, 2-norm and max-norm shown for both methods of limiting, original shown as solid line order of accuracy 1.0 - 1.4, modified shown as (+, 2-norm) and (*,max-norm) order of accuracy .6 - 1.0.

Figure 3.7 shows the order of accuracy for the numerical solution shown in figure 3.6. With the use of flux-limiters we see that the order of accuracy of the solution method diminishes as expected. While figure 3.5 shows that without the use of limiters the method is second-order accurate, figure 3.7 shows that with the use of limiters the accuracy falls to about 1.5 for the original method and 1.0 for the modified method.

Note that figure 3.6 shows the smoothing effect expected with the use of flux limiters. Also note that in most of the accuracy plots two limiting methods are compared. These two methods are the original limiting method implemented in CLAWPACK, introduced in Section 2.2, and the transmission based limiting method which will be discussed in Section 4.2.

In figure 3.7 we saw that for smooth data without discontinuities the two limiting methods had an order of accuracy between 1.5 (original method) and 1.0 (modified method). Figure 3.9 shows the order of accuracy for the two methods in the presence of a single discontinuity, see figure 3.8. From figure 3.9 we can see that when a discontinuity exists within the medium, the order of accuracy of the two limiting methods falls to about 1.2 for the original method and 0.8 for the modified method.

Thus for smooth data in a discontinuous medium we expect that with the use of limiters our numerical methods will be somewhat less than first order accurate. Now that we have demonstrated CLAWPACK'S performance on a single interface, we will address the question of multiple interfaces, or discontinuities.

3.2 Several Interfaces

Before exploring questions of homogenization, possibly involving hundreds of interfaces, we would first like to study CLAWPACK'S performance on the modeling of several interfaces. We first extend the solution method to the case where we have many interfaces, but we have not yet reached a situation in which homogenization theory is applicable. Figures 3.10-3.13 show the results of running the forward problem on a region with 10 different layers of medium.

In each figure we have four levels of discretization for identical initial pulses in identical domains. The coarsest level divides the interval $[0, 1]$ into 100 grid points,

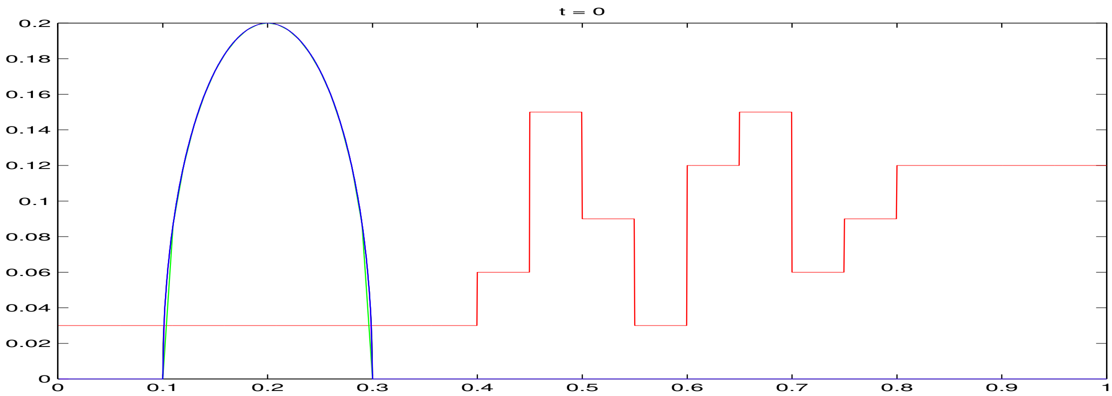

Figure 3.10: initial pressure pulses, time=0, N=100,500,1000,2000

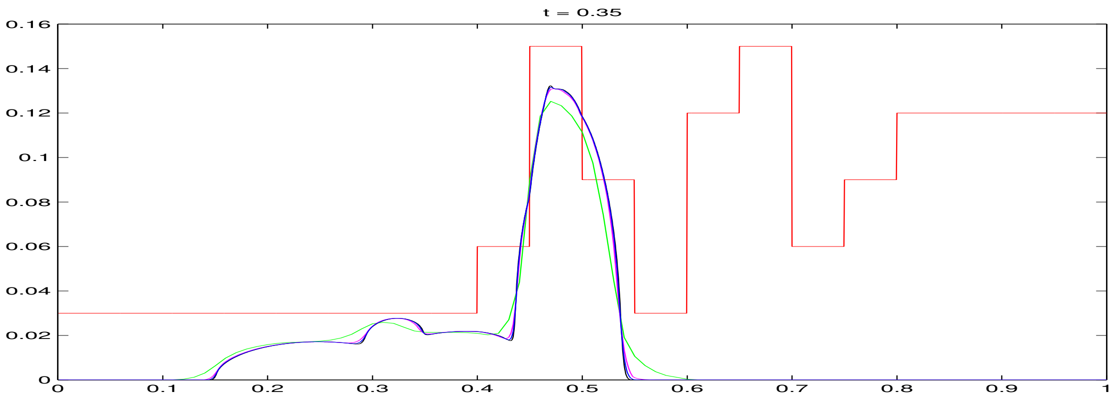

Figure 3.11: pressure at time=0.35, N=100,500,1000,2000

thus with the pulse width of .2 we get 20 grid points per pulse width for this level of refinement. Finer levels of refinement have $N = 500, 1000,$ and 2000. From the figures, one can see that for the coarsest level of refinement the solution suffers from numerical diffusion. Also, one can see that once we have 50 grid points per pulse width, i.e. the second level of refinement, very little is gained by further levels of refinement.

As with the single interface problem we would like to know the order of accuracy of the method. Figure 3.15 shows the order of accuracy found for the two methods of

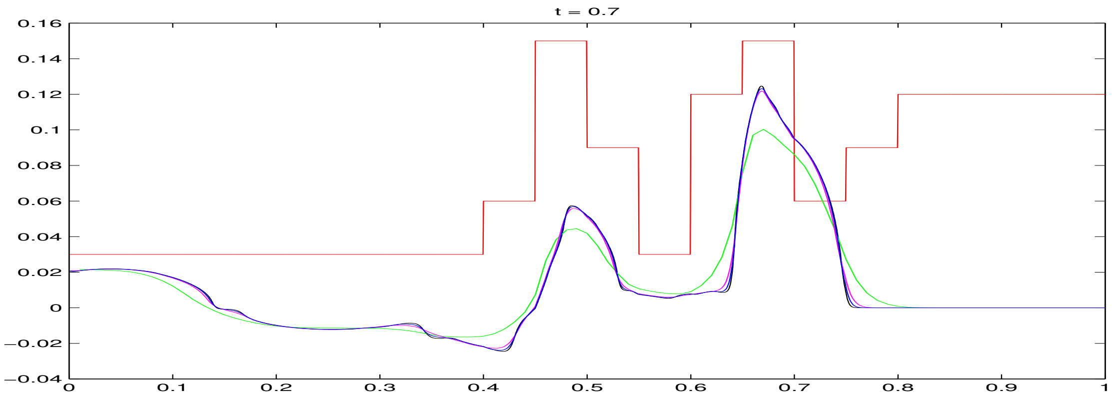

Figure 3.12: pressure at time=0.7, N=100,500,1000,2000

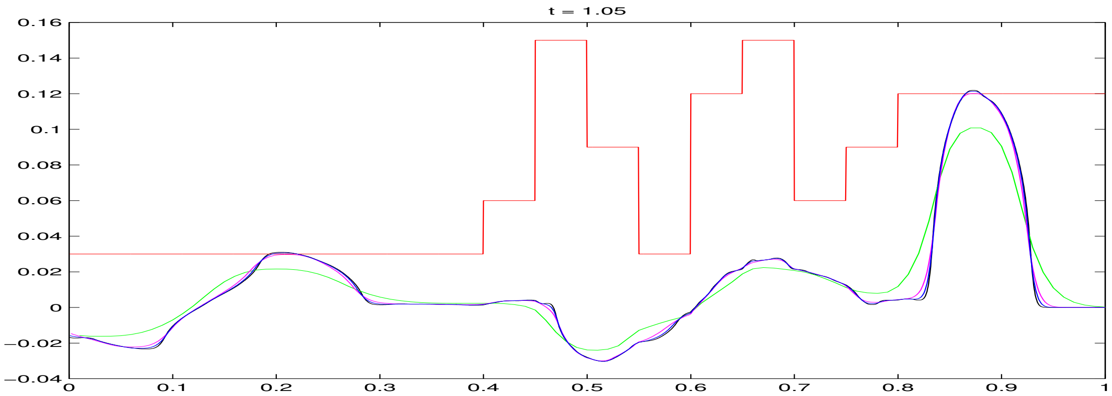

Figure 3.13: pressure at time=1.05, N=100,500,1000,2000

limiting applied to smooth data in a medium with 10 interfaces, figure 3.14. As with the single interface, the original method of limiting converges a rate of about 1.1 and the modified method of limiting converges with a rate near 0.8.

3.3 Periodic medium

The following will be an effort to verify results given in [15]. We assume a medium which has material properties that are periodic with period $2\pi\gamma$, i.e. the medium is made up of cells with size $2\pi\gamma$. Then ρ and μ satisfy the following: $\rho(x+2\pi\gamma) = \rho(x)$

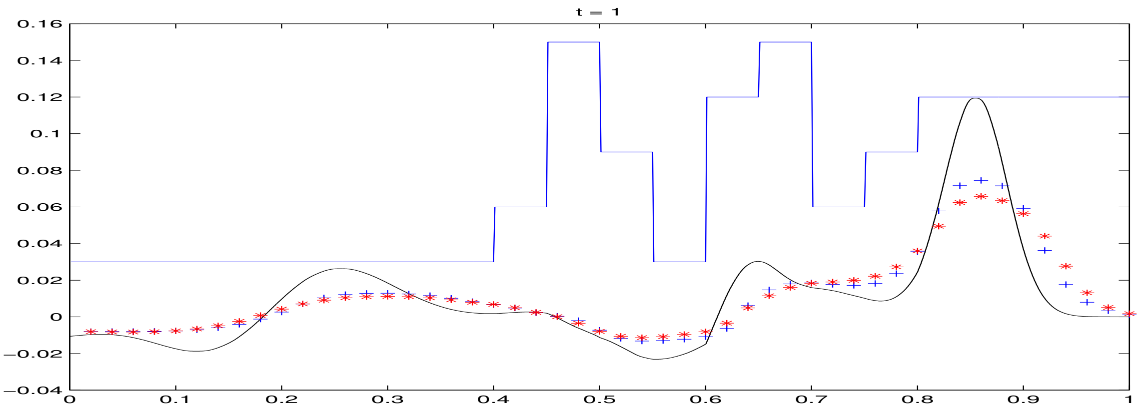

Figure 3.14: $\triangle t < \triangle x$ original and modified limiters used, numerical solutions shown for N=50, original(+) and modified(*) methods, with “reference”solution at N=1600. Smooth data in a region with 10 interfaces.

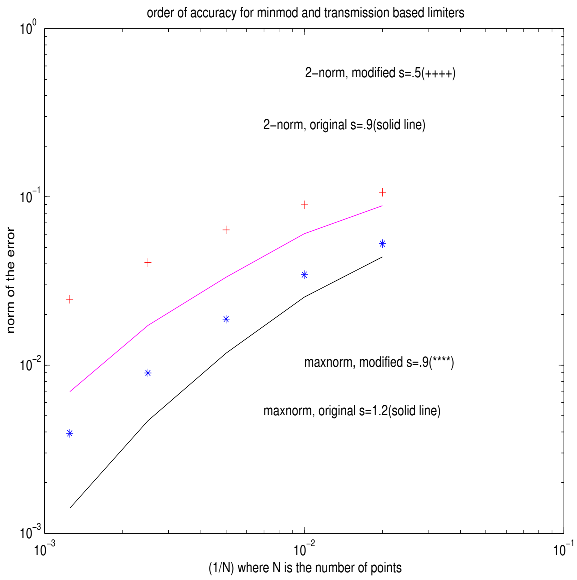

Figure 3.15: Order of accuracy for numerical solutions of figure 3.14. N=50,100,200,400,800 are compared with numerical solution at N=1600, 2-norm and max-norm shown for both methods of limiting, original shown as solid line, modified shown as (+, 2-norm) and (*,max-norm), order of accuracy near .8 for modified method and 1.1 for original method.

and $\mu(x+2\pi\gamma) = \mu(x)$. Given the system stated above (1.16 and 1.17) p, the pressure, can be eliminated to find the following equation for u

$$\rho(x)u_{tt}(x,t) = (\mu(x)u_x(x,t))_x. \tag{3.2}$$

We will solve (3.2) with initial data $u(x,0) = f(x)$ and $u_t(x,0) = 0$. To make use of the following expansion procedure we will also assume that $f(x)$ is band-limited,

$$f(x) = \frac{1}{2\pi}\int_{\xi \le K} F(\xi)e^{i\xi x}d\xi,$$

so that the shortest wavelength of the Fourier components of $f(x)$ is $\lambda = 2\pi/K$. We then find an approximate solution to $u(x,t)$ with the assumption that $\epsilon = 2\pi\gamma/\lambda \ll 1$. Thus if the frequency, λ^{-1} of the initial data $f(x)$ is much greater than the period of the medium, we will have a valid solution.

For a complete discussion of Bloch expansion theory see [1] and [14]. Given a periodic, heterogeneous medium we would like to find the dispersion relation for a propagating wave. Bloch or Floquet expansion gives parameters which effectively characterize the average effects of a periodic, heterogeneous medium. I.e the Bloch expansion procedure effectively homogenizes the medium. An effective dispersion relation for the homogenized medium can be found.

To make the analysis more tractable, as is most often done (see [6] and [7]), we assume steady oscillatory waves of frequency $\omega_0(k)$, and a time dependence of $e^{(-i\omega_0(k)t)}$, so we can replace $(u(x,t), p(x,t))$ in (1.15) by $e^{i\omega_0(k)t}(u(x), p(x))$. Thus equation (3.2) simplifies to

$$-\omega_0^2\rho(x)u(x) = (\mu(x)u_x(x))_x. \tag{3.3}$$

By Floquet's Theorem, there are solutions of (3.3) of the form

$$u(x) = v(x)e^{ikx}, \tag{3.4}$$

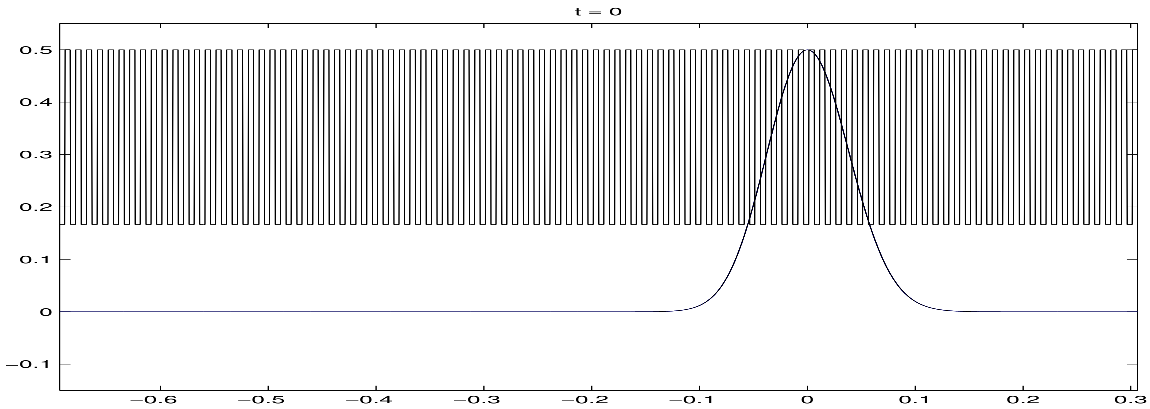

Figure 3.16: density profile and initial position of right-going pulse, time=0, N=4000. Note that in this and the following figures the density and bulk modulus profile is scaled by 1/6. The density is periodic with a value of either $\rho = 1$ or $\rho = 3$ and $\mu = \rho$ everywhere.

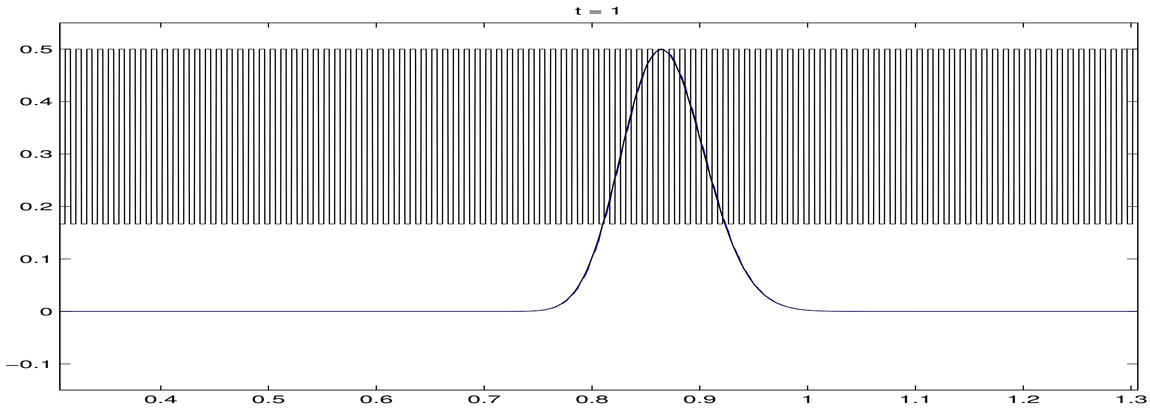

Figure 3.17: comparison of "exact" solution with $\triangle t = \triangle x$ and "numerical" solution with $\triangle t < \triangle x$, right-going pulses, original limiter, time=1, N=4000.

where $v(x)$ is periodic of period $2\pi\gamma$ and k is the wave number. Solutions for $u(x,t)$ in (3.2) are known as Bloch or Floquet waves. Bloch waves may be evaluated over a single cell, of length $a = 2\pi\gamma$, via equation (3.3) with periodic boundary conditions

$$u(a/2) = u(-a/2)e^{ika},$$

and

$$u'(a/2) = u'(-a/2)e^{ika}.$$

The solution for all x can then be found by the recurrence relation

$$u(x+a) = u(x)e^{ika}.$$

If we assume a solution of the form (3.4) and substitute into (3.3) then

$$\frac{\partial}{\partial x} \to \frac{\partial}{\partial x} + ik,$$

and we are left with the following eigenvalue problem for v

$$\left(\frac{\partial}{\partial x} + ik\right)\left[\mu(x)\left(\frac{\partial}{\partial x} + ik\right)v(x)\right] = -\omega_0^2(k)\rho(x)v(x).$$

Here v are the eigenfunctions corresponding to the eigenvalues ω_0^2. This eigenvalue problem can be used to find, via a Taylor's expansion of $\omega_0(k)$ at $k = 0$, an expression for the new effective dispersion relation of the pulse in the homogenized medium, given by

$$\omega_0(k) = \Omega_1 k + (1/6)\epsilon^2\Omega_3 k^3 + \cdots \tag{3.5}$$

Thus as $\epsilon \to 0$ we have an effective medium propagation vector given by $\omega_0(k) = \Omega_1 k$. Here Ω_1 is the effective speed of the homogenized medium given by

$$\Omega_1^2 = \left[\bar{\rho}\left(\overline{\frac{1}{\mu}}\right)\right]^{-1}.$$

Note that this effective wave speed is given by the usual formula $c = \sqrt{\mu/\rho}$ but using the average of ρ and the harmonic average of μ over the interval.

If this line of analysis is continued one can derive the governing equation in "homogenized" form as

$$u_{tt} = \Omega_1^2 u_{xx} + \frac{\Omega_1 \Omega_3}{3} a^2 u_{xxxx}, \tag{3.6}$$

recall that $a = 2\pi\gamma$ is the period. See [15] for details. This homogenized equation has no term of order ϵ, is dispersive, and fourth order in x. Note that this same equation is derived in [6] via multiple scale techniques. We will return to a discussion of this second homogenization theory in Section 6.1.

In [15], results were found for the following experimental set up

$$\rho(x) = \begin{cases} \rho_1 = 1 = \mu_1, & \text{for } 0 < x < 2\pi\theta\gamma \\ \rho_2 = 3 = \mu_2, & \text{for } \ 2\pi\theta\gamma < x < 2\pi\gamma \end{cases}$$

where θ is the volume fraction of the mixture. In this experiment $\theta = 0.5$ and the period is set at $\gamma = 0.5$ also. For this case we find that

$$\Omega_1^2 = \left[\bar{\rho}\left(\overline{\frac{1}{\mu}}\right)\right]^{-1} = 2/(2(1+1/3)) \ \Rightarrow \Omega_1 = 0.8660.$$

The authors in [15] chose this specific case because the wave speed c is constant throughout the medium. Although the density and bulk-modulus are varying periodically, they are chosen in such a way that $c = 1$ everywhere. This set-up was chosen so that the method of characteristics could be used. To use the method of characteristics, implemented by the authors in [15], one must always choose $\triangle t = \triangle x$. Although CLAWPACK has no such restriction on the choice of $\triangle t$ and $\triangle x$, if $\triangle t = \triangle x$ then, for this example, the method of solution implemented by CLAWPACK reduces to the method of characteristics.

To replicate the results found in [15] via CLAWPACK, we input the given density and bulk modulus and solve problem with a large Gaussian velocity pulse and a very

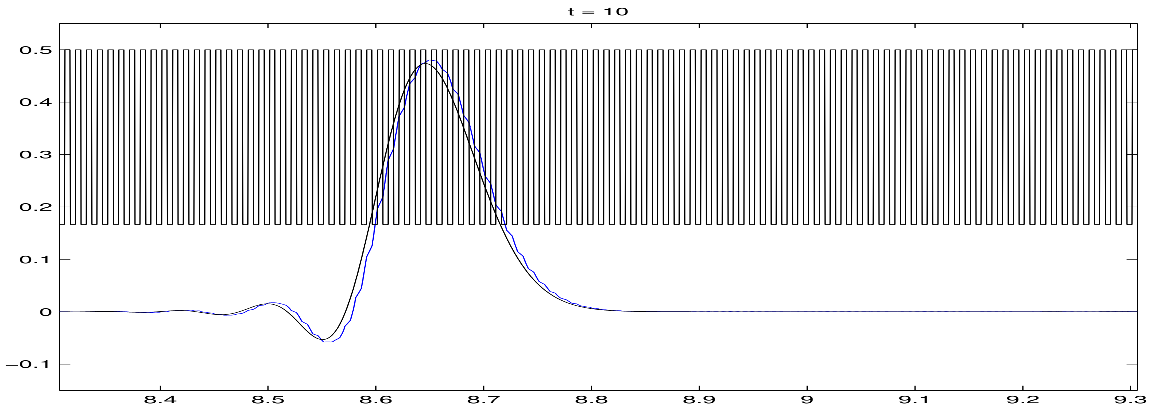

Figure 3.18: comparison of “exact” solution with $\triangle t = \triangle x$ and “numerical” solution with $\triangle t < \triangle x$, right-going pulses, original limiter, time=10, N=4000. Note that much better results can be obtained with the modified limiter, see figure 3.20.

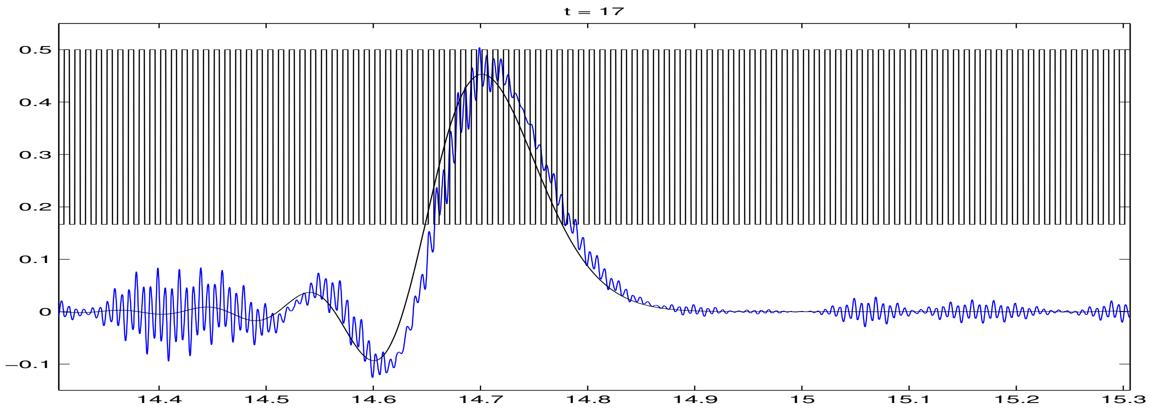

Figure 3.19: comparison of “exact” solution with $\triangle t = \triangle x$ and “numerical” solution with $\triangle t < \triangle x$, right-going pulses with numerical instability, original limiter, time=17, N=4000. Note that much better results are obtained with modified limiter, see figure 3.21.

small period (so that $\epsilon \approx 0$). If CLAWPACK is successful than we should see that that the pulse travels with an effective speed of $c_{\text{eff}} = 0.8660$. A simple way to test this is to let the pulse advect with periodic boundary conditions until it has traveled 1 time unit. If the pulse is traveling at the correct speed then the distance traveled should be .866, or after traveling for 10 time units the pulse should move a distance of 8.66. Figures 3.16-3.18 show that CLAWPACK reproduces the expected effective

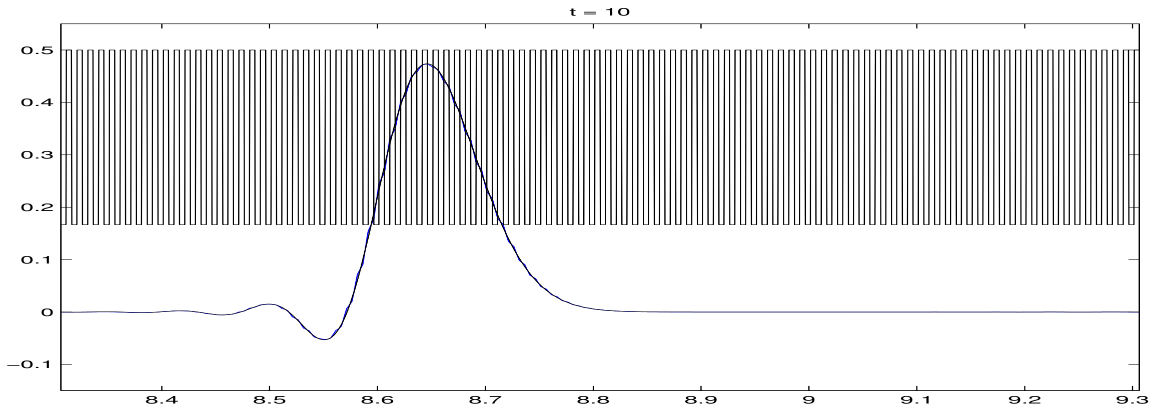

Figure 3.20: comparison of “exact” solution with $\triangle t = \triangle x$ and “numerical” solution with $\triangle t < \triangle x$, right-going pulses, modified limiter, time=10, N=4000.

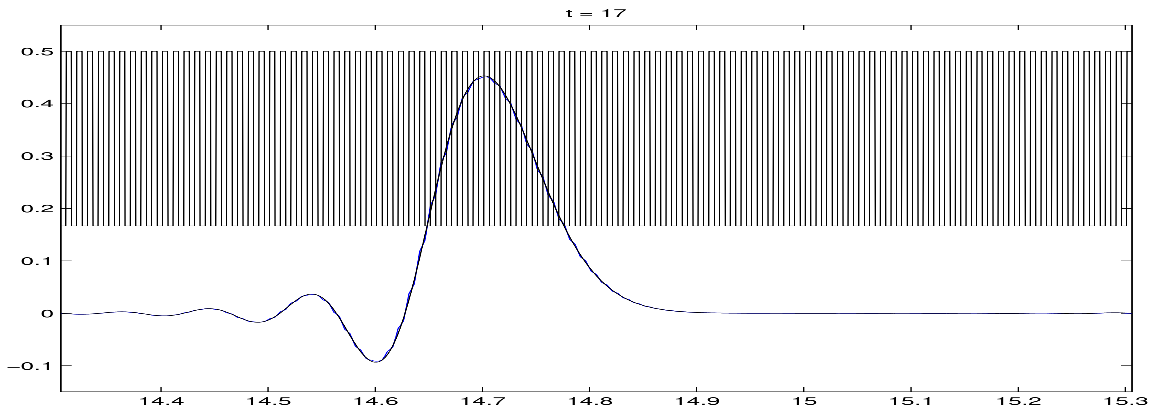

Figure 3.21: comparison of “exact” solution with $\triangle t = \triangle x$ and “numerical” solution with $\triangle t < \triangle x$, right-going pulses, modified limiter, time=17, N=4000.

propagation speed.

Note that even though the sound speed is constant everywhere, the medium is still dispersive. There is an impedance contrast across interfaces separating layers of different material parameters, see Section 3.1. Thus from equation (3.5) we expect the wave to suffer from dispersion for nonzero Ω_3. In this example $\Omega_3 = -.01353$. In addition to the effective wave speed, figures 3.18- 3.21 show the effective dispersion of the homogenized medium. It should be clear that this dispersion is physical and not a numerical artifact.

If we run the problem for a much longer time we experience a severe numerical instability. (see figure 3.19) The investigation and resolution (see figures 3.21 and 3.20) of this instability will be explored in Section 4.

Chapter 4

TRANSMISSION BASED LIMITERS

4.1 Failure of standard limiters

In the example discussed in Section 3.3, we see that the numerical solution with the minmod limiter is only valid for a short time. The medium in this example is characterized by many layers of material of a given impedance $Z = \rho c$. The layers are arranged so that to the left and right of each layer is an interface which separates the layer from a layer of different impedance. The layers are repetitive in nature so that for a layer of impedance $Z = 1$, the layers to the left and right will be of impedance $Z = 3$. As discussed previously, for this example we always have $\rho = \mu$ so that within each layer $c = 1$.

The problem is initialized by creating a Gaussian velocity pulse within the periodic medium on a large domain. The pulse splits with half of the perturbation energy traveling each direction. When the two pulses are separated, the right-going pulse is used as initial data in the computational domain. Periodic boundary conditions are imposed and the pulse is allowed to advect to the right.

As the pulse advects, it is continuously moving into layers of different impedance. As discussed in Section 3.1, each time the pulse moves into a region of different impedance, the pulse is partially transmitted and partially reflected. In this example, as is necessary for the prediction of an effective wave speed, the pulse-width is much greater than the width of a single layer of the medium. As the pulse advects a distance equal to the width of a single layer, the entire area within the pulse encounters one of the many interfaces contained within the pulse-width. Thus the entire pulse is constantly undergoing multiple, internal transmissions and reflections at the many interfaces contained within the pulse. These transmissions and reflections must interact in such a way that a right-going pulse remains a right-going-only pulse. From figures 3.16-3.18 we can see that for a short time a right-going pulse does indeed remain a right-going-only pulse.

As stated previously the medium in this example is constructed so that $\rho = \mu$ everywhere, i.e. in each layer $c = 1$. Thus if we choose $\triangle t = \triangle x$, (see Section 3.3) then in a single time step $\triangle t$, the waves $\mathcal{W}_i^p$ propagate a distance of one grid cell ($\triangle x$). In this case, for a given time step, the value of the solution in cell i is an exact combination of the waves $\mathcal{W}_i^2$ and $\mathcal{W}_{i+1}^1$ generated in the previous time step. As a consequence of choosing $\triangle t = \triangle x$, with $c = |\lambda_i^p| = 1$ in each layer, the "second-order" terms in equation (2.3) drop out and the upwind method reduces to the method of characteristics. It should be clear that in this case the waves are not limited.

If $\triangle t = \triangle x$, for this example, the solution is solved exactly and the pulse advects to the right with no left-going reflections. If $\triangle t < \triangle x$, than as the pulse advects to the right the tail-end of the pulse generates very small left-going disturbances at each interface. If flux-limiters are not used the left-going disturbances die out quickly as they advect to the left. However, if flux-limiters are used the left-going disturbances are effectively advected to the left.

In order to advect the right-going pulse for a long time we have had to use periodic boundary conditions. Thus while the pulse under investigation advects to the right, the left-going disturbances advect to the left and interfere with each other. While the periodic boundary conditions allow the left-going disturbances to remain in the domain, they are in no way responsible for creating the disturbances, see figure 4.2. Although the left-going disturbances are very small in amplitude, they have the same frequency as the medium. The long term interaction of the left-going disturbances with the medium leads to a resonant effect. The resonating signal eventually grows in amplitude so that, in the periodic domain, the right-going pulse is completely

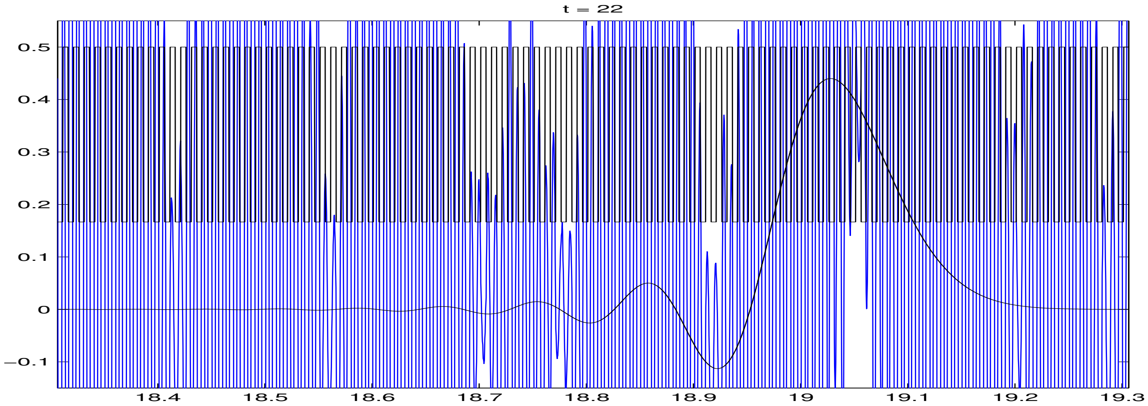

Figure 4.1: comparison of "exact" solution with $\triangle t = \triangle x$ and "numerical" solution with $\triangle t < \triangle x$, right-going pulses with numerical instability, original limiter, time=22, N=4000.

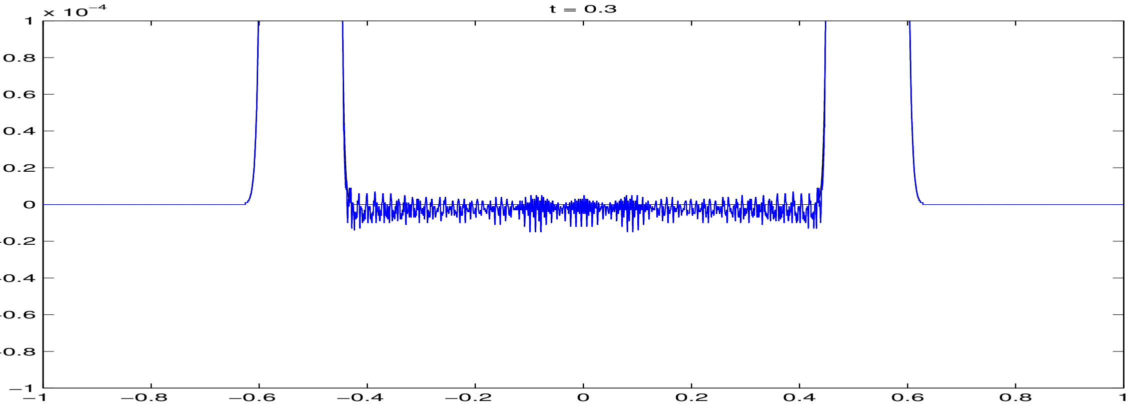

Figure 4.2: comparison of "exact" solution with $\triangle t = \triangle x$ and "numerical" solution with $\triangle t < \triangle x$, left and right-going pulses with numerical instability, original limiter, time=0.3, N=4000, Note the scale of the disturbances.

degraded, see figure 4.1. Note that as in figures 3.16-3.19, the density profile has been scaled by 1/6.

The left-going disturbances are generated by the tail-end of the pulse as it advects to the right. We believe that these disturbances are caused by the failure of the flux-limiter to properly describe the transmitted and reflected parts of the waves $\mathcal{W}_i^p$ as they move through an interface. Recall that for $\triangle t = \triangle x$ the waves $\mathcal{W}_i^p$ advect one grid-cell each time step. As interfaces in the medium are at grid points, if $\triangle t = \triangle x$, the waves $\mathcal{W}_i^p$ are never advected partially through an interface. However

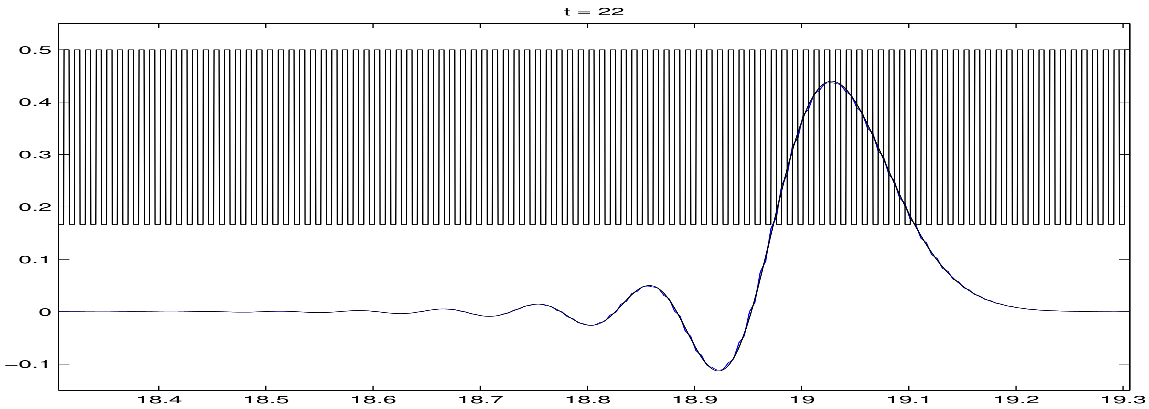

Figure 4.3: comparison of “exact” solution with $\triangle t = \triangle x$ and “numerical” solution with $\triangle t < \triangle x$, right-going pulses, modified limiter, time=22, N=4000.

if $\triangle t < \triangle x$, then a wave $\mathcal{W}_i^p$ generated from a grid point next to an interface is only partially advected through the interface, in the next time step. A wave advected part way through an interface should be partially transmitted and partially reflected, see Section 3.1. Thus proper limiter implementation in the presence of a discontinuous medium should account for the effects of partial transmission at interfaces.

4.2 Revision of limiters

In order to modify the limiting method we must know the transmission and reflection coefficients, for a wave moving in either direction, at each interface. These coefficients are easily computed via (3.1). Recall equation (2.9) as

$$\theta_i^p = \frac{W_{i-1}^p \cdot W_i^p}{W_i^p \cdot W_i^p}. \tag{4.1}$$

Now consider the case when $\lambda_i^p > 0$ so that $\mathcal{W}_i^p$ is advected to the right. In the following time step, only the transmitted part of the right-going wave will move into the cell $[x_i, x_{i+1}]$. Thus instead of only comparing $\mathcal{W}_i^p$ with $\mathcal{W}_{i-1}^p$, as in (4.1) we must compare $\mathcal{W}_i^p$ with the transmitted part of $\mathcal{W}_{i-1}^p$. To incorporate these ideas into the existing CLAWPACK framework we can alter (4.1) in the following manner.

After all the waves $\mathcal{W}_i^p$ have been computed we can define a separate set of waves $\mathcal{W}_c^p$. If we first consider $p = 1$, so that $\lambda_i^1 = -c_{i-1} < 0$, then we must compare $\mathcal{W}_i^1 = \alpha_i^1 r_{i-1}^1$ with $\mathcal{W}_{i+1}^1 = \alpha_{i+1}^1 r_i^1$. However, we want to compare with the part of $\mathcal{W}_{i+1}^1$ which will be transmitted in the next time step. Thus we decompose $\mathcal{W}_{i+1}^1$ into the eigenvectors characterizing the interface on which $\mathcal{W}_{i+1}^1$ will be incident

$$\mathcal{W}_{i+1}^1 = \alpha_{i+1}^1 r_i^1 = \mathcal{B}_{i+1}^1 r_{i-1}^1 + \mathcal{B}_{i+1}^2 r_i^2. \tag{4.2}$$

Solving for $\mathcal{B}_{i+1}^1$ and $\mathcal{B}_{i+1}^2$ we find

$$\mathcal{B}_{i+1}^1 = \alpha_{i+1}^1 \left(\frac{2\rho_{i-1}c_{i-1}}{\rho_{i-1}c_{i-1} + \rho_i c_i} \right) = \alpha_{i+1}^1 \left(\frac{2Z_2}{Z_1 + Z_2} \right) = \alpha_{i+1}^1 \mathcal{T}_{i,l}, \tag{4.3}$$

$$\mathcal{B}_{i+1}^2 = \alpha_{i+1}^1 \left(\frac{\rho_{i-1}c_{i-1} - \rho_i c_i}{\rho_{i-1}c_{i-1} + \rho_i c_i} \right) = \alpha_{i+1}^1 \left(\frac{Z_2 - Z_1}{Z_1 + Z_2} \right) = \alpha_{i+1}^1 \mathcal{R}_{i,l}. \tag{4.4}$$

Here $\mathcal{T}_{i,l}$ and $\mathcal{R}_{i,l}$ are the transmission and reflection coefficients of a left-going wave incident on an interface at the grid point x_i, see Section 3.1. Given (4.3) and (4.4) we define

$$\mathcal{W}_c^1 = \alpha_{i+1}^1 \mathcal{T}_{i,l} r_{i-1}^1 \frac{\triangle t}{\triangle x}. \tag{4.5}$$

For $p = 2$, we have $\lambda_i^2 = +c_i > 0$, an analogous argument holds and we find

$$\mathcal{W}_{i-1}^2 = \alpha_{i-1}^2 r_{i-1}^2 = \mathcal{B}_{i-1}^1 r_{i-1}^1 + \mathcal{B}_{i-1}^2 r_i^2, \tag{4.6}$$

where

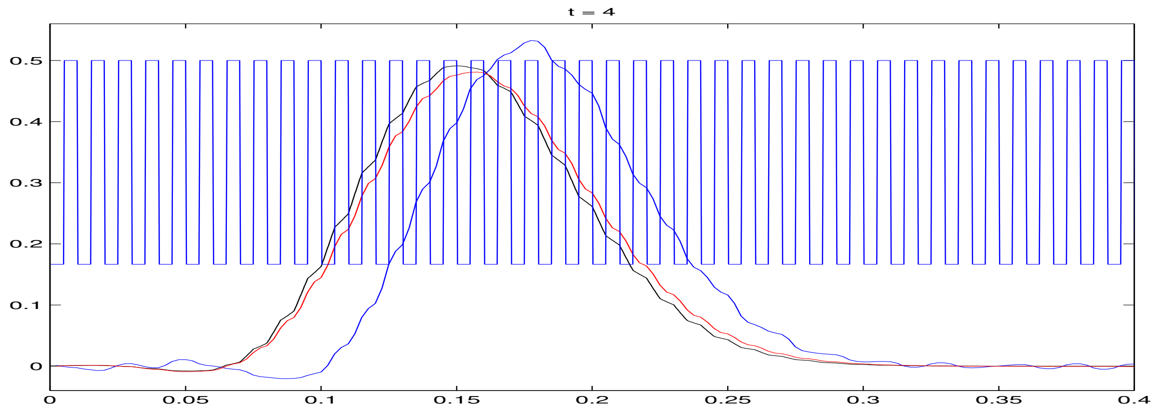

Figure 4.4: $\triangle t < \triangle x$ original and modified limiters used, numerical solutions shown for N=400, original and modified methods, with "reference" solution at N=6400. Note that the large variation between numerical solutions and "reference" solution is due to the large variation in resolutions. I.e. N=6400 for reference and N=400 for numerical solutions. Note also that the "reference" solution is the most leftward pulse while the solution obtained with the original method is the most rightward pulse.

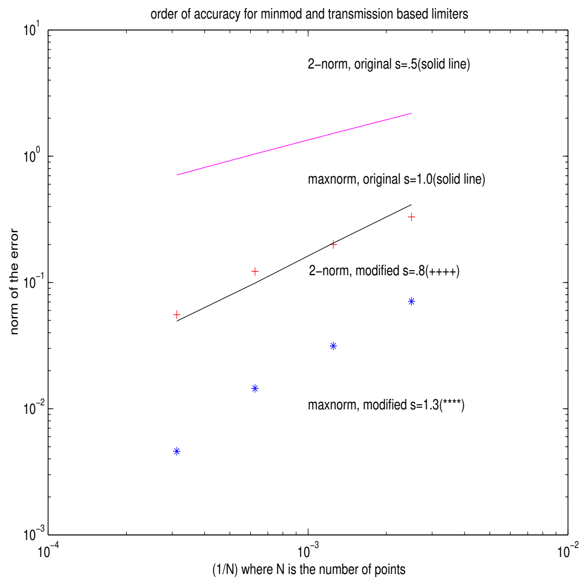

Figure 4.5: Order of accuracy for numerical solutions of figure 4.4. N=400,800,1600,3200 are compared with numerical solution at N=6400, 2-norm and max-norm shown for both methods of limiting, original shown as solid line, modified shown as (+, 2-norm) and (*,max-norm), order of accuracy near 1.1 for modified method and 0.8 for original method.

$$\mathcal{B}^1_{i-1} = \alpha^2_{i-1}\left(\frac{\rho_i c_i - \rho_{i-1}c_{i-1}}{\rho_{i-1}c_{i-1} + \rho_i c_i}\right) = \alpha^2_{i-1}\left(\frac{Z_2 - Z_1}{Z_1 + Z_2}\right) = \alpha^2_{i-1}\mathcal{R}_{i,r}, \tag{4.7}$$

$$\mathcal{B}_{i-1}^2 = \alpha_{i-1}^2 \left(\frac{2\rho_i c_i}{\rho_{i-1}c_{i-1} + \rho_i c_i} \right) = \alpha_{i-1}^2 \left(\frac{2Z_2}{Z_1 + Z_2} \right) = \alpha_{i-1}^2 \mathcal{T}_{i,r}. \tag{4.8}$$

We define the comparison wave as

$$\mathcal{W}_c^2 = \alpha_{i-1}^2 \mathcal{T}_{i,r} r_i^2 \frac{\triangle t}{\triangle x}. \tag{4.9}$$

Here $T_{i,r}$ and $R_{i,r}$ are the transmission and reflection coefficients for a right-going wave incident on the same interface. Now we redefine (4.1) as

$$\theta_i = \frac{\mathcal{W}_c^p \cdot \mathcal{W}_c^p}{W_i^p \cdot W_i^p}, \tag{4.10}$$

where $\mathcal{W}_c^p$ is given in (4.5) for $\lambda_i^p < 0$, and $\mathcal{W}_c^p$ is given in (4.9) for $\lambda_i^p > 0$. Note that $\mathcal{W}_c^p$ and $\mathcal{W}_i^p$ are now linearly dependent so that we are just comparing magnitudes.

When this simple change in the definition of θ_i^p is implemented in the preceding example, the resonant effect observed in figures 3.19 and 4.1 is completely eliminated. Figure 4.3 shows that a right-going pulse can be advected to the right (apparently indefinitely) with no disruptive numerical artifacts. Although results are not shown, this redefinition of θ_i^p appears to be valid for all limiters implemented by CLAWPACK. Note also that the dispersion seen in the profile of the advected pulse is expected, see Section 5.1.

In addition to more accurately solving the problem, this redefinition of the limiting method allows us to claim that the scheme is now positive. See [13] for a definition of positivity and proof of positivity for this form of θ_i. At present the implications of this need to be explored further. We will return to a short discussion of positivity in Section 6.1.

Now that we have a robust numerical solution method we are free to explore applications which, to our knowledge, have not been numerically solvable, see Section

5. Before moving to these new applications we will give an order of accuracy study for both the new (4.10) and old (4.1) methods of flux-limiting.

Figure 4.5 shows the order of the accuracy of the two limiting methods shown in figure 4.4. We find that for the original method of limiting the order of accuracy is near 0.8 and for the modified method the order is near 1.1. If we recall the order of accuracy of the methods in previous examples we see that for the periodic medium the order of accuracy of the methods has changed dramatically. In all previous examples the original method has consistently converged faster than the modified method, while for the periodic medium the modified limiting method converges faster. While figure 4.4 clearly shows that modified limiting method more accurately solves the problem, the reason for the change in the order of accuracy of the two methods remains unclear. A theoretical explanation for the differences seen in the two limiting methods may be possible to explain by a multiple scale analysis of the modified equations. We will return to this idea later in Section 6.1.

Chapter 5

NEW APPLICATIONS

5.1 Constant impedance - no dispersion

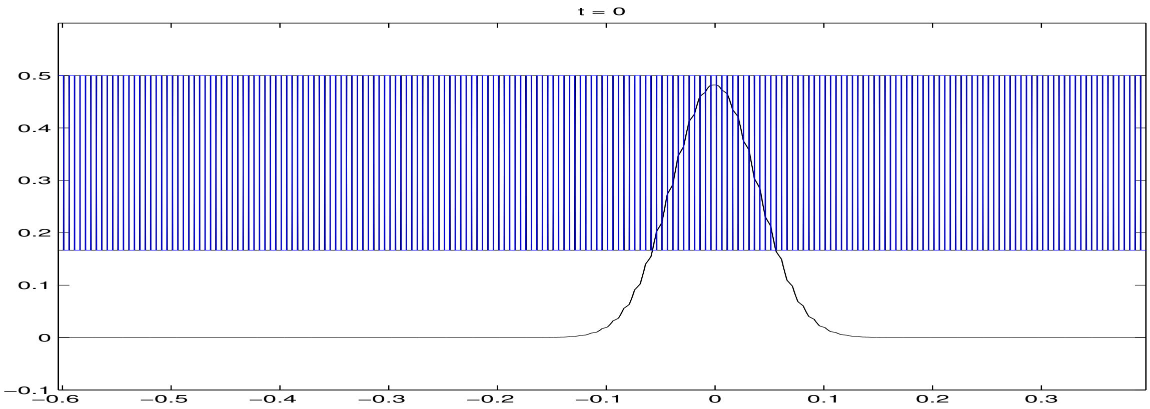

Figure 5.1: $\triangle t < \triangle x$ right-going pulse in non-dispersive medium, modified limiter, time=0, N=4000.

In Section 3.3 homogenization theory was used to determine an effective wave speed in a periodic, dispersive medium. Homogenization theory also predicts that for a periodic medium with no impedance contrast, the medium will be non-dispersive, see [15] . Given a heterogeneous periodic medium with $Z_1 = Z_2$, an advecting pulse should move through the medium at the predicted effective wave speed, without dispersion.

To create such a medium we set

$$\rho(x) = \begin{cases} \rho_1 = 1 \text{ and } \ \mu_1 = 9, & \text{for } 0 < x < 2\pi\theta\gamma \\ \rho_2 = 3 \text{ and } \ \mu_2 = 3, & \text{for } \ 2\pi\theta\gamma < x < 2\pi\gamma \end{cases}$$

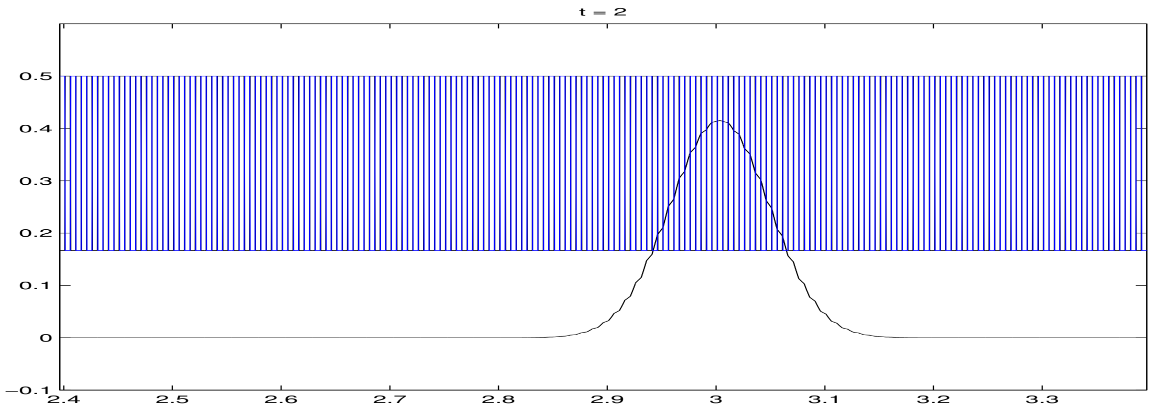

Figure 5.2: $\triangle t < \triangle x$ right-going pulse in constant impedance medium, modified limiter, time=2, N=4000.

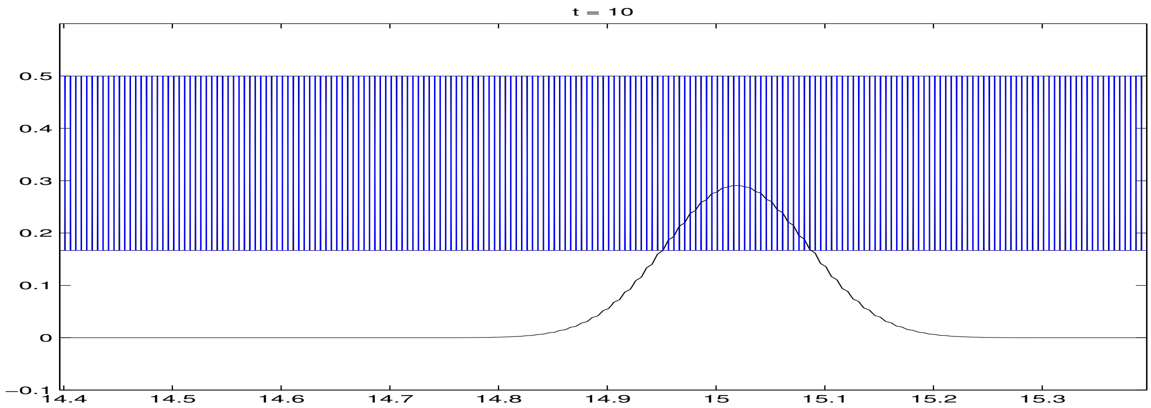

Figure 5.3: $\triangle t < \triangle x$ right-going pulse in constant impedance medium, modified limiter, time=10, N=4000.

where θ is the volume fraction of the mixture. In this experiment, as before $\theta = 0.5$ and the period is set with $\gamma = 0.5$. This gives an impedance of $Z_1 = Z_2 = 3$ in the entire medium, while within the layers the wave speed is either $c = 3$ or $c = 1$. Thus the wave advects in different layers of medium with a different speed c_i. However since there is no impedance contrast there should not be any reflections or refractions at the interfaces between layers.

We use the same procedure outlined in Section 3.3 to find an effective wave speed

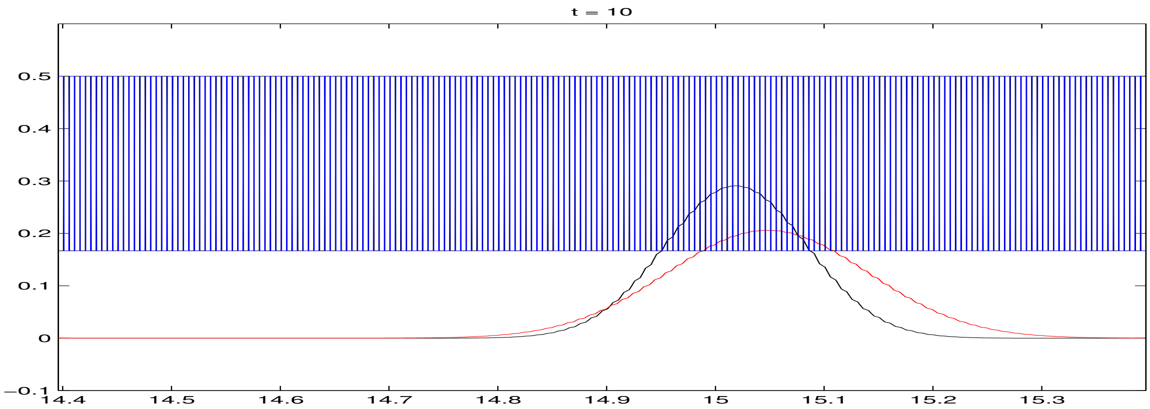

Figure 5.4: $\triangle t < \triangle x$ right-going pulses in constant impedance medium, modified limiter, time=10, N=4000 and N=1600.

as

$$\Omega_1 = \frac{3}{2}. \tag{5.1}$$

Figures 5.1-5.3 clearly show that the effective wave speed is demonstrated. We can see that after traveling for 10 time units the pulse has moved a distance of 15. Also it is shown that the medium appears to be non-dispersive.

As the pulse advects it does appear to suffer from dissipation, a numerical effect that is not characteristic of the medium. Figure 5.4 shows the pulse after it has advected the same medium at different levels of refinement. Further study of this problem is needed. A good test we hope to make is to study this type of medium on a non-uniform grid. Thus even though the wave speed is different from layer to layer, with a non-uniform grid we should be able to set $c \triangle t = \triangle x$, see Section 6.1.

5.2 Stochastic homogenization

Consider an acoustic wave, of short wavelength, propagating in a random medium which deviates only slightly from a uniform medium. As in the periodic medium we would like to find effective parameters which characterize the random medium.

Two very useful parameters we would like to find are the phase and amplitude of a wave advecting in the random medium. To solve for the amplitude, as well as for the polarization and the phase, we can use a perturbation expansion in powers of the magnitude of the non-uniformity of the medium. See [2] for details.

As in section 3.3, we begin with (3.2) as

$$\rho(x)u_{tt} = (\mu(x)u_x)_x. \tag{5.2}$$

Again, we assume a time harmonic solution of the form $e^{ikt}(u(x), p(x)) = (u(x,t), p(x,t))$ such that (5.2) reduces to

$$-k^2\rho(x)u = (\mu(x)u_x)_x. \tag{5.3}$$

To this point we have only been studying the one-dimensional acoustics problem. However, the following analysis is quite general and we will not assume any restriction to one dimension. Effective parameters will be found for the three-dimensional case. We can then use these parameters when we return to one-dimension.

If a constant bulk modulus, μ, is assumed, then variation in the sound speed, or index of refraction of the medium, will be a function of the density, ρ. Under this condition the 3-d version of (5.3) can be rewritten as the following Helmholtz equation;

$$[\triangle + k^2 n^2(\mathbf{x})]u(\mathbf{x}, k) = 0, \tag{5.4}$$

where $n(\mathbf{x}) = \sqrt{\rho/\mu}$ is the refractive index and k is the wave number. Note that (5.4) is not restricted to 1 dimension. We assume that the medium is nearly constant (we can take this to be 1), so that the index of refraction has the form

$$n(\mathbf{x}) = 1 + \epsilon\beta(\mathbf{x}), \tag{5.5}$$

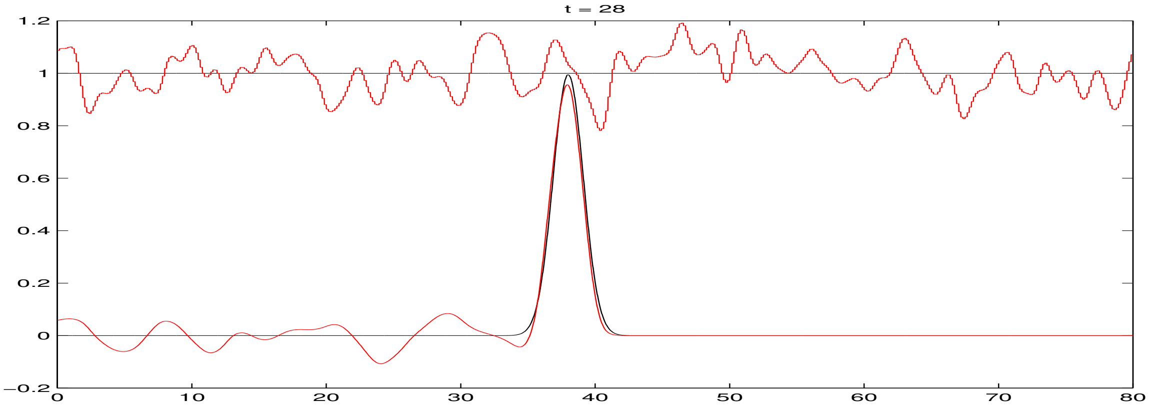

Figure 5.5: right-going pulses in a constant and correlated random index of refraction, time=28, wave speeds of mediums plotted to scale near the top, N=5120.

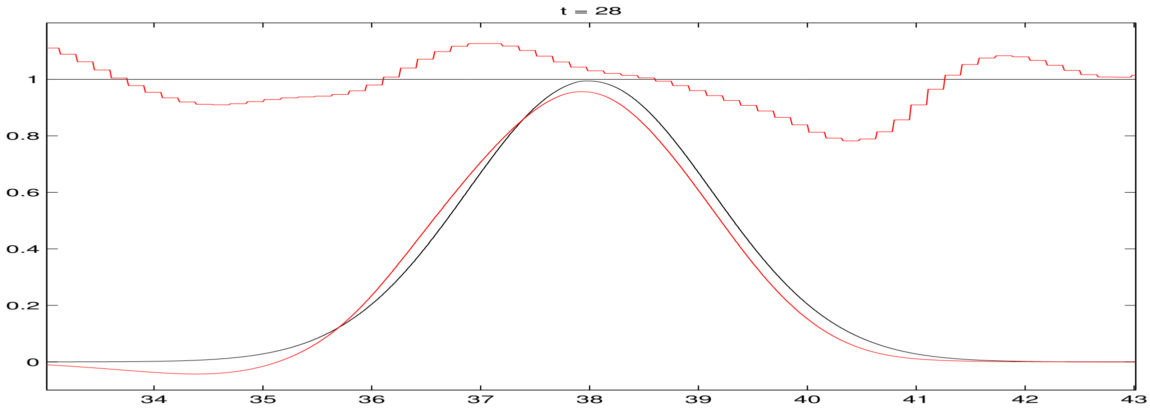

Figure 5.6: close up of right-going pulses in a constant and correlated random index of refraction, time=28, wave speeds of mediums plotted to scale near the top, N=5120.

where ϵ is a small parameter and β is a function characterizing the deviation from a homogeneous medium. Note that this definition of the index of refraction is equivalent to a variable sound speed c given by

$$c^{-1}(\mathbf{x}) = 1 + \epsilon\beta(\mathbf{x}). \tag{5.6}$$

For large k, i.e. short wavelength, seek an asymptotic expansion of u, of the form;

$$u(\mathbf{x}, k) = e^{[ikS(\bar{r})][A(\mathbf{x})+(ik)^{-1}A^1(\mathbf{x})+O(k^{-2})]}, \tag{5.7}$$

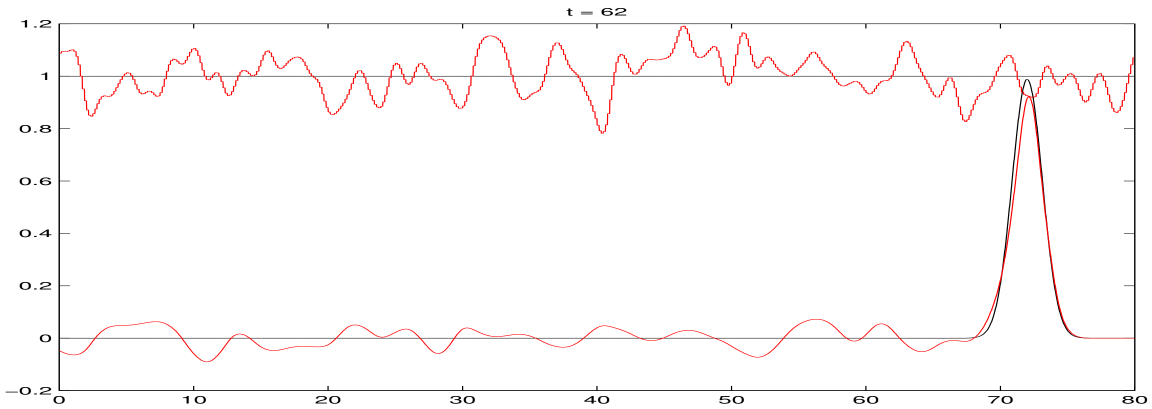

Figure 5.7: right-going pulses in a constant and correlated random index of refraction, time=62, wave speeds of mediums plotted to scale near the top, N=5120.

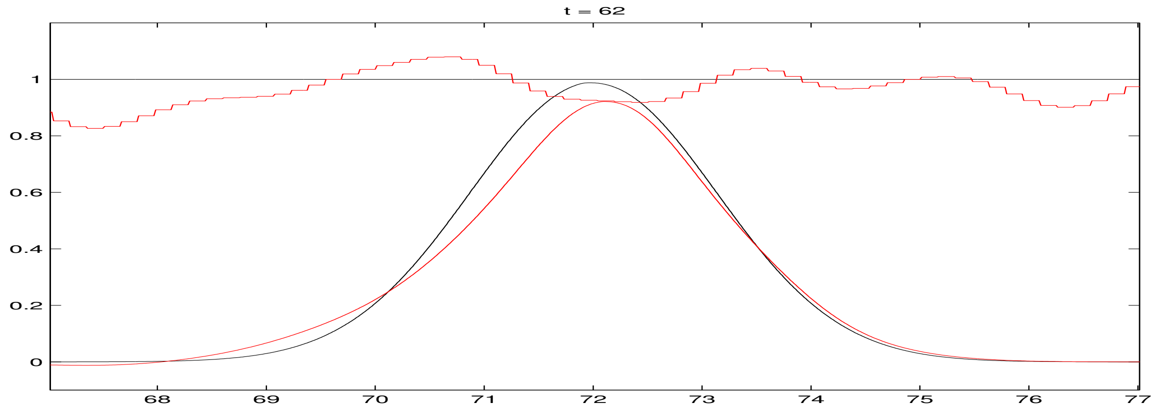

Figure 5.8: close up of right-going pulses in a constant and correlated random index of refraction, time=62, wave speeds of mediums plotted to scale near the top, N=5120.

where S is the phase and A is the amplitude of the wave, u. If S and A are expanded in powers of ϵ and (5.7) is substituted into (5.4), with (5.5), then like coefficients of ϵ can be equated to find the expansions of S and A. For details of these methods, see [5] and [4], also for stochastic applications, see [16].

Given a plane-wave moving to the right, i.e. toward increasing values of x, in a region where n is given as (5.5), S and A can be found as

$$S(\mathbf{x}, \epsilon) = x + \epsilon \int_0^x \beta(t, y, z)dt - \frac{\epsilon^2}{2} \int_0^x \left[\int_0^t \nabla_T \beta(\tau, y, z)d\tau\right]^2 dt + O(\epsilon^3).$$

$$A(\mathbf{x},\epsilon) = 1 + \frac{\epsilon}{2}\left[\beta(0,y,z) - \beta(x,y,z) - \int_0^x (x-t) \bigtriangleup_T \beta(t,y,z,)dt\right] + O(\epsilon^2),$$

where $\bigtriangledown_T$ is the gradient operator transverse to the x direction. Using these expressions for S and A in (5.7) gives u with an error of $O(\epsilon^2) + O(k^{-1}) + O(k\epsilon^3)$.

Assume that $\beta(\mathbf{x})$ is a random function, which satisfies

$$\langle\beta(\mathbf{x})\rangle = 0, \quad \langle\beta(\mathbf{x}_1)\beta(\mathbf{x}_2)\rangle = \langle\beta^2\rangle N(|\mathbf{x}_1 - \mathbf{x}_2|),$$

where $N(s)$ is an isotropic two-point correlation function. We assume the $N(s)$ is very small for $s > l$, where l is the correlation length of the medium. Since β is random, S, A and u are also random and the correlation function can be defined via

$$\langle\bigtriangledown_T\beta(t,y,z)\cdot\bigtriangledown_T\beta(s,y,z))\rangle = -2\langle\beta^2\rangle N'(|t-s|)|t-s|^{-1}. \tag{5.8}$$

With the use of (5.8) the mean of the amplitude and the mean of the phase, of the plane wave, can be found as

$$\langle A(\mathbf{x},\epsilon)\rangle = 1 + O(\epsilon^2),$$

and for $x \gg l$

$$\langle S(\mathbf{x},\epsilon)\rangle \sim x - \epsilon^2 x^2 D, \tag{5.9}$$

where

$$D = -\langle\beta^2\rangle \int_0^\infty N'(s)s^{-1}ds.$$

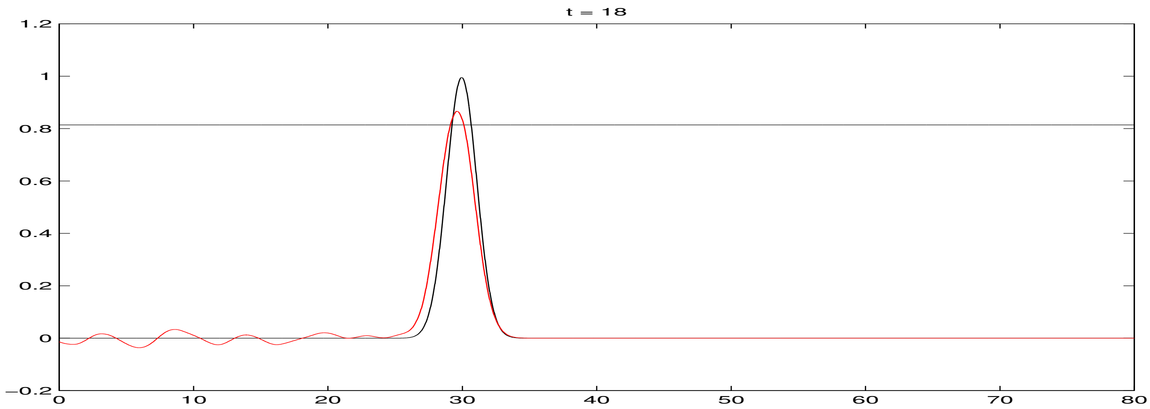

Figure 5.9: right-going pulses in a constant density and uncorrelated random density , time=18, density of mediums shown only in close up, N=5120.

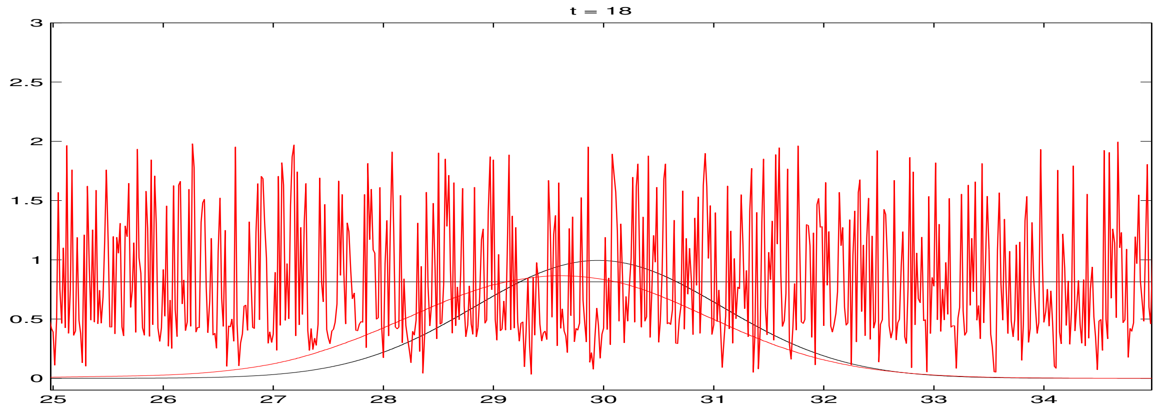

Figure 5.10: close up of right-going pulses in a constant density and uncorrelated random density, time=18, density of mediums plotted to scale, N=5120.

From (5.9), the effective wave speed c_{eff}, in the random medium, can be calculated. Given that $\langle S(\mathbf{x})\rangle = xc_0/c_{\text{eff}}$, where c_0 is the wave speed in the unperturbed medium, we find

$$c_{\text{eff}} = \frac{c_0}{1-\epsilon^2 Dx} \sim c_0(1+\epsilon^2 Dx). \tag{5.10}$$

This shows that, so long as we have a valid perturbation result i.e. $\epsilon^2 x \ll 1$, c_{eff} increases linearly with x.

In 1 dimension, there is no transverse direction to x, so that

$$\nabla_T \beta = 0 \rightarrow \quad \langle S(\mathbf{x}, \epsilon) \rangle = x,$$

which implies, that in 1 dimension, $c_{\text{eff}} = c_0$. To test this result we will initialize a right-going pulse in a medium where the wave speed c is defined as $c(x) = 1 + \epsilon\beta(x)$. Assuming a Gaussian wave pulse, where β has a Gaussian correlation function, if suitable values of $\epsilon, l,$ and x are chosen, we expect to find the effective wave speed c_{eff} as c_0. Figures 5.5-5.8, show that a wave propagating in the stochastic medium does indeed move with $c_{\text{eff}} = c_0$. For these examples the values of $\epsilon, l,$ and x were chosen to be $\epsilon = 1/25, l = 1,$ and $x = 80$. The function β had 512 random numbers with a mean of .023 and a standard deviation of 1.96. The resolution was such that there were 5120 grid points in the domain, so that the wave speed was constant over distances of 10 grid cells. Note that CLAWPACK also gives an excellent solution of the acoustics problem in an uncorrelated random medium, even with with very large variations in material parameters, see figures 5.9-5.10. At present we are unaware of any other numerical solver which is capable of solving such problems. The more interesting case of 2-dimensions, i.e. where the effective wave speed increases with distance, is currently under investigation.

Chapter 6

CONCLUDING REMARKS

6.1 *Future Work*

Throughout this presentation we mentioned several areas of possible further investigation. One area of interest which has yet to be explored is "capacity-form flux differencing". As previously stated we can write the acoustics equations as

$$\begin{bmatrix} 1/\mu(x) & 0 \\ 0 & \rho(x) \end{bmatrix} \begin{bmatrix} p \\ u \end{bmatrix}_t + \begin{bmatrix} 0 & 1 \\ 1 & 0 \end{bmatrix} \begin{bmatrix} p \\ u \end{bmatrix}_x = 0. \tag{6.1}$$

We define the functions which pre-multiply q_t as capacity functions $\kappa^1(x) = 1/\mu(x)$ and $\kappa^2(x) = 1/\rho(x)$. Note that this has no relation to the κ associated with isentropic flow in Section 1.2. In this form we see that the solution of the Riemann problem always gives two identical waves which travel with speed ± 1 regardless of material parameters in the cell. If we recall the update formula, in the absence of limiters, we must replace (2.3) with

$$F^{LW}(q_i) = F^{up}(q_i) - \frac{\triangle t}{2 \triangle x} \left(\sum_{p=1}^{M_w} (1 - \frac{\triangle t}{\kappa^p_{i-1/2} \triangle x}) \mathcal{W}^p_{i+1} - \sum_{p=1}^{M_w} (1 - \frac{\triangle t}{\kappa^p_{i-1/2} \triangle x}) \mathcal{W}^p_i \right). \tag{6.2}$$

Here $\kappa^p_{i-1/2}$ is the appropriate average or harmonic average of κ^p_i and κ^p_{i-1}. Exactly how formulation of the problem in this manner will affect solutions and limiting methods is unclear and remains an unanswered question which we hope to pursue.

As mentioned in Section 1.3, for variable material parameters we do not have strict conservation form. In consequence, even for smooth data q, the second-order corrections in the update formula are not correct. The numerical methods implemented by CLAWPACK give the proper second-order correction terms for constant-coefficient matrices. We have seen that this is true in figures 3.8 and 3.9. If the matrix $A(x)$ in (1.16) is constant, then the derivative of $A(x)$ is zero. For this case it can be shown that CLAWPACK is second-order accurate, see [12]. However when $A(x)$ is not constant then derivatives of $A(x)$ exist and, as is discussed in [12], the update formula is no longer second order accurate. The proper way to define second-order corrections, especially in the presence of flux-limiters, for a variable coefficient $A(x)$ also remains to be seen.

In Section 4.2 we briefly mentioned "positivity". We believe that the modified version of the flux-limiter gives a method which is "positive". In [13] positivity is defined in such a way that any conservative numerical scheme which is positive has bounded growth in the l^2 norm. We would like to explore this connection in the future to see if it can be shown that numerical method with modified limiting is a stable algorithm.

In a medium of constant impedance we found that our scheme appeared to be numerically dissipative. A medium of this type should not be dissipative. Also our scheme did not appear to cause numerical dissipation in any of the other types of media studied. Clearly the cause of this numerical dissipation must be investigated. In this effort we hope to use a non-uniform grid, so that in every cell we can set $c \triangle t = \triangle x$. In a non-uniform grid formulation we expect that we will be able to solve the problem exactly via the method of characteristics. Thus we will have an "exact" solution to compare with that given by our numerical method. In this setting we should be able to more readily understand the cause of the observed numerical dissipation.

As we mentioned previously, one homogenization theory which gives a "homogenized" equation for a heterogeneous periodic medium is multiple scale analysis, see [6]. In this work we have found that CLAWPACK can directly solve the acoustics equations to replicate solution behavior predicted by homogenization theory. Also in the course of this investigation we found that, for the heterogeneous periodic medium, a severe numerical instability developed. Although we are able to correct this instability by alterations to the limiting method, we are not able to theoretically predict the instability. Nor are we presently able to theoretically explain how the modified limiting method actually prevents the instability. We hope to explore these questions via study of what is known as the "modified equation".

A numerical method attempts to approximately solve a given "exact" equation. However, what actually happens is that the numerical method "exactly" solves an equation which may or may not be a good approximation to the "exact" equation we wish to solve. One tool for analyzing the behavior of a numerical method is to derive the equation which the numerical method is actually solving. This equation is known as the modified equation. Thus we plan to continue this work by finding the correct modified equation and using a multiple scale analysis to find theoretical explanations for the observed behavior of the two limiting methods.

6.2 Conclusions

CLAWPACK has been used to successfully reproduce expected theoretical results for acoustics in a heterogeneous periodic medium. We have shown that CLAWPACK can numerically verify effective media parameters and wave propagation characteristics predicted by homogenization theory. The flux-limiting method originally implemented by CLAWPACK has been observed to fail in the periodic heterogeneous medium. In this case a modified transmission based limiting method corrected the failure. We have verified that CLAWPACK can reproduce existing theoretical and numerical results and numerically solve problems previously beyond the reach of numerics. Thus we have shown that the numerical methods utilized by CLAWPACK are an excellent tool for testing homogenization theories. In the future we also hope to show that homogenization theory can provide a means of studying the theory related to these numerical methods.

BIBLIOGRAPHY

[1] A. Bensoussan, J.L. Lions, and G. Papanicolaou. *Asymptotic Analysis for Periodic Structures*. North-Holland, Amsterdam, 1978.

[2] William Boyse and Joseph B Keller. Short acoustic, electromagnetic, and elastic waves in random media. *J. Opt. Soc. Am. A*, 12:380,389, Febuary 1995.

[3] William C. Elmore and Mark A. Heald. *Physics of Waves*. Dover, 1985.

[4] Jr. Frank C. Karal and Joseph B. Keller. Elastic, electromagnetic, and other waves in a random medium. *Journal of Mathamatical Phusics*, 5(4), 1964.

[5] Joseph B. Keller. Stochastic equations and wave propagation in random media. In *Proceedings of Symposia in Appl. Mathematics*, volume 16, 1964.

[6] J. Kevorkian and D.L. Bosley. Multiple scale homogenization for weakly nonlinear conservation laws with rapid spatial fluctuations. Department of Applied Mathematics, University of Washington, Submitted.

[7] E. H. Lee and Wei H. Yang. On waves in composite material with periodic structure. *SIAM J. Appl. Math.*, 25:492–499, November 1973.

[8] Randall J. Leveque. Clawpack – a software package for solving multi-dimensional conservation laws. To appear in, Proceedings of the 5th International Conference on Hyperbolic Problems, Stony Brook, June 1994.

[9] Randall J. Leveque. Note 13. CLAWPACK, 1995.

[10] Randall J. Leveque. High-resolution conservative algorithims for advection in incompressible flow. *SIAM J. Num. Anal.*, 33:627–665, 1996.

[11] Randall J. Leveque. Numerical methods for conservation laws and hyperbolic systems. Lecture Notes, 1996.

[12] Randall J. Leveque. Wave propagation algorithims for multi-dimensional hyperbolic systems. To appear in, J. Comput. Phys., 1996.

[13] Xu-Dong Liu and Peter D. Lax. Positive schemes for sloving multi-dimensional hyperbolic systems of conservation laws. submitted to CFD Journal, Jan 1995.

[14] Enrique Sanchez-Palencia. *Non-Homogeneous Media and Vibration Theory.* Springer-Verlag,Berlin Heidelberg New York, 1980.

[15] F. Santosa and W. W. Symes. A dispersive effective medium for wave propagation in periodic composits. *SIAM J. Appl. Math.*, 51:984–1005, 1991.

[16] Kazimierz Sobczyk. *Stochastic Wave Propagation.* PWN-Polish Scientific Publishers–Warszawa, 1985.

[17] W. W. Symes. Mathematics of reflection seismology. To appear in, Mathematical Frontiers in Reflection Seismology, Not yet published.